Trapping and near-trapping by arrays of cylinders in waves

D. V. EVANS and R. PORTER
School of Mathematics, University Walk, University of Bristol, Bristol, BS8 1TW, U.K.
e-mail: d.v.evans@Bristol.ac.uk

Abstract. In this paper, some recent developments and new results concerning the trapping of waves by arrays of vertical circular cylinders is presented. In particular, the cases are examined when there is a circular arrangement of cylinders and both finite and infinite periodic linear arrays of identical cylinders. Only for the infinite array is there pure trapping of waves – known as Rayleigh–Bloch or edge waves – which, for particular dominant wavenumbers, reduce to the well-known trapped-mode solutions for a cylinder between two parallel walls having either Neumann or Dirichlet conditions upon them. This latter case is considered separately and some new results are presented. In the circular array and finite linear array the concept of near-trapping is introduced where large resonant motions are found to occur at certain frequencies of the incident wave field. In the case of the finite linear array, these near-trapping frequencies are related to the Rayleigh–Bloch trapped-wave frequencies for the infinite array. Finally, the case when there are two or more lines of cylinders in the linear array is examined.

Keywords: trapping, water waves, cylinders, wavemaker, Rayleigh–Bloch.

1. Introduction

The classical linear theory of water waves has proved extremely successful in predicting the forces on fixed or moving structures in low amplitude waves and forms the basis for such considerations in ocean engineering and related fields.

The simplest, and the only explicit solution, in three dimensions, involving a fixed structure is the solution derived by McCamy and Fuchs [1] for the total wave field due to a long-crested wave in water of finite depth h, incident upon a bottom-mounted surface-piercing fixed rigid circular cylinder, extending Havelock's (1929) infinite-depth wavemaker theory. The solution, for example, for the first-order exciting forces on the cylinder turns out to be an infinite series of Hankel functions. See Mei [3, pp. 312–315] for details. The reasons why this problem permits an explicit solution are two-fold. First, since the cross-section of the cylinder is constant with depth and the cylinder is fixed, the dependence on depth z of the velocity potential describing the flow can be extracted via a multiplicative term $\cosh \kappa (h + z)$ where κ is the positive root of $\omega^2 = g\kappa \tanh \kappa h$, thereby reducing the problem to a solution of the Helmholtz equation in two-dimensions with a Neumann condition on the circle $r = a$ (we have assumed the circle, of radius a, has its centre at the origin of Cartesian co-ordinates x, y with $x = r \cos \theta$, $y = r \sin \theta$). The second reason is that the incident wave potential can be expressed in polar co-ordinates as an infinite sum of a product of Bessel and trigonometric functions enabling the Neumann condition to be satisfied on $r = a$ explicitly.

It is natural to consider how this solution can be extended. Clearly, the depth dependence can be extracted for any number of fixed vertical cylinders of arbitrary cross-section extending throughout the depth. Also, if they are circular, the Graf addition theorem for Bessel func-

tions can be used to shift co-ordinates between cylinders. This device enables the problem of the scattering by arbitrary arrays of circular cylinders to be reduced to the solution of a rapidly-converging infinite system of equations for certain Fourier coefficients A_n^k related to the expansion of the field in the vicinity of, say, the kth cylinder. This idea was used by Twersky [4], whilst Linton and Evans [5], unaware of Twersky's work, re-derived the theory and also showed how the potential on any cylinder could be expressed simply in terms of an infinite series involving the A_n^k, whilst the exciting forces depended only on A_1^k and A_{-1}^k.

The Linton and Evans [5] theory is the starting point for the present paper and is summarized in Section 2. In Section 3 we consider a circular configuration of cylinders and consider how the exciting forces on each cylinder differs from the force on a single cylinder predicted by the McCamy and Fuchs [1] results. The relevance to the wave forces on the supporting columns of an offshore drilling platform is clear, but there are undoubtedly other industrial applications involving the solution of the Helmholtz equation in the domain exterior to a circular array of circular cylinders.

It is shown that the exciting force increases dramatically as the spacing between each of four identical circular cylinders, placed at the four corners of a square, is reduced. We term this phenomenon near-trapping and show that it arises because of the existence of standing waves trapped in the interior region bounded by the cylinders whose energy slowly leaks away to infinity. A general consideration of this effect is presented. In particular, we show, by destroying the symmetry of the circular arrangement, whilst not increasing the gaps between adjacent cylinders, that the effect disappears showing that this phenomenon is not simply a manifestation of the large resonant oscillations which can occur within a harbour connected to the open sea by a narrow entrance when excited by an incident wave field of appropriate frequency.

In Section 4 the theory is applied to a linear periodic array of cylinders in a manner similar to Maniar and Newman [4] and this part of the paper has much in common with their work. They showed how the forces on the centre cylinders in a large linear array of identical cylinders became large at certain frequencies of the incident wave field which correspond to the trapped modes which can exist in the vicinity of a circular cylinder confined between two parallel walls on which either a Neumann or a Dirichlet condition is applied. Such trapped modes in the Neumann case were first discovered by Callan *et al.* [7]. In the present paper we show how, by increasing indefinitely the number of cylinders, dropping the incident wave, and assuming a Bloch or Floquet-type expansion for the wave field, an infinite system is obtained whose solution describes Rayleigh–Bloch waves which are confined to the vicinity of the line of cylinders and decay to zero in a direction normal to this line. For a discussion of Rayleigh–Bloch waves in the context of diffraction gratings, see Wilcox [8].

When the dominant wavenumber β in the Rayleigh–Bloch expansion takes particular values, the solution reduces to standing waves along the infinite array which, just as in Maniar and Newman [6], can be interpreted as trapped modes of either Neumann or Dirichlet type around a single cylinder confined between parallel walls.

For other values of β we demonstrate that the Rayleigh–Bloch solution is connected to the near-trapping of waves arising in a corresponding finite periodic linear array of cylinders as shown by Maniar and Newman [6]. This conclusion is important in enabling the prediction of large forces on finite arrays of cylinders to be made on the basis of results for infinite arrays which are usually easier to determine. The results of Section 4 are new.

We return, in Section 5, to the original formulation of Callan *et al.* [7], but we now allow the possibility of both Dirichlet and Neumann modes above the lowest point of the corresponding

continuous spectrum and also allow the possibility of modes which can be either symmetric or antisymmetric about a plane through the centre of the cylinder normal to the channel walls. We find new antisymmetric Neumann modes below the cut-off and a single Dirichlet and Neumann mode above the cut-off at a precise value unique cylinder to channel width ratio.

It is clear that knowledge of the trapped modes which can exist near a single cylinder in a channel is important in predicting the large forces on cylinders near the centre of a long single linear array of cylinders. However, in many applications at least a double linear array of cylinders would be needed as, for example, the supports of an offshore runway. It is therefore important to predict the corresponding trapped mode frequencies for two or even more cylinders on the channel centreplane. This is considered in Section 6 where results for the special case of two identical cylinders are discussed.

2. Formulation

We use classical linear water-wave theory in which we seek a harmonic velocity potential $\Phi(x, y, z, t)$. The formulation follows that of Linton and Evans [5] where the velocity potential Φ is expressed as

$$\Phi(x, y, z, t) = \mathrm{Re}\{\phi(x, y) \cosh \kappa(z + h) \, \mathrm{e}^{-\mathrm{i}\omega t}\}, \tag{2.1}$$

where $\omega/2\pi$ is the wave frequency, h the depth of water and κ is the positive root of

$$\omega^2 = g\kappa \tanh \kappa h. \tag{2.2}$$

Then ϕ satisfies

$$(\nabla^2 + \kappa^2)\phi(x, y) = 0 \tag{2.3}$$

exterior to the cylinders and

$$\frac{\partial \phi}{\partial n} = 0 \tag{2.4}$$

on each cylinder.

We assume there are N circular cylinders having arbitrary position and radius and write

$$\phi(x, y) = \phi_{\mathrm{inc}}(x, y) + \sum_{j=1}^{N} \phi_s^j(x, y), \tag{2.5}$$

where

$$\phi_{\mathrm{inc}}(x, y) = \mathrm{e}^{\mathrm{i}\kappa r \, \cos(\theta - \theta_{\mathrm{inc}})} = I_k \, \mathrm{e}^{\mathrm{i}\kappa r_k \cos(\theta_k - \theta_{\mathrm{inc}})} \tag{2.6}$$

and

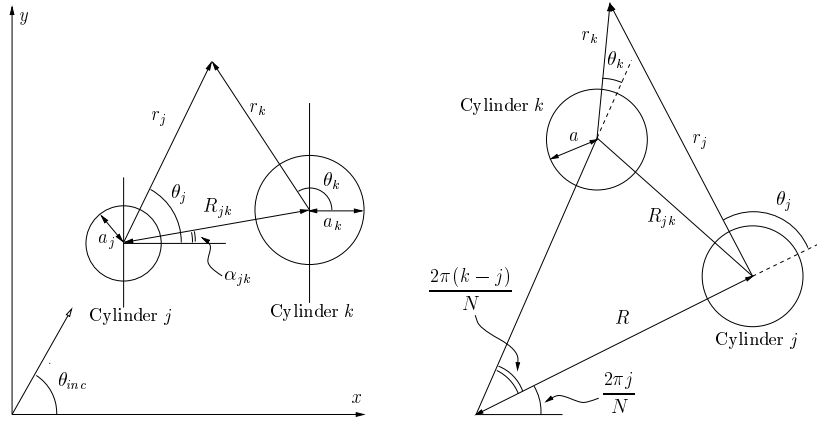$$I_k = \mathrm{e}^{\mathrm{i}\kappa(x_k \cos \theta_{\mathrm{inc}} + y_k \sin \theta_{\mathrm{inc}})}. \tag{2.7}$$

Figure 1. The co-ordinate system of Linton and Evans [5] and for the cylindrical array.

Thus, the incident wave makes an angle θ_{inc} with the x-direction and cylinder k has centre (x_k, y_k). The general form for the scattered potential from cylinder j is

$$\phi_s^j = \sum_{n=-\infty}^{\infty} A_n^j Z_n^j H_n(\kappa r_j) \, e^{in\theta_j}, \tag{2.8}$$

where

$$Z_n^j = J_n'(\kappa a_j)/H_n'(\kappa a_j)$$

and a_j is the radius of cylinder j. Here $H_n \equiv J_n + i Y_n$ is the Hankel function of the first kind. By using Graf's addition formula, Linton and Evans [5] showed that to satisfy (2.4) then the coefficients A_m^k must satisfy

$$A_m^k + \sum_{\substack{j=1 \\ \neq k}}^{N} \sum_{n=-\infty}^{\infty} A_n^j Z_n^j \, e^{i(n-m)\alpha_{jk}} H_{n-m}(\kappa R_{jk}) = -I_k \, e^{im(\pi/2-\theta_{\text{inc}})}$$

$$k = 1, \dots, N, \quad -\infty < m < \infty. \tag{2.9}$$

Here R_{jk} is the distance between the centres of cylinders j and k, and α_{jk} is the angle between the line from the centre of cylinder j to the centre of cylinder k and the positive x-direction. Notice that the effect of the incident wave is included through the term θ_{inc} on the right-hand side.

It was shown in Linton and Evans [5] that the total potential may be expressed in the coordinates of cylinder j, say, as simply

$$\phi(r_j, \theta_j) = \sum_{n=-\infty}^{\infty} A_n^j F_n(\kappa r_j) \, e^{in\theta_j}, \quad r_j < R_{jk} \; \forall k, \tag{2.10}$$

where

$$F_n(\kappa r_j) = Z_n^j H_n(\kappa r_j) - J_n(\kappa r_j) \tag{2.11}$$

and where r_j, θ_j are polar coordinates measured from the centre of cylinder j in the positive x-direction. From the above equation, the first-order exciting force on the jth cylinder can be derived. Thus

$$\frac{X^j}{F^j} = -\frac{1}{2}\begin{Bmatrix} i \\ 1 \end{Bmatrix}\left(A^j_{-1}\begin{Bmatrix} - \\ + \end{Bmatrix}A^j_1\right), \tag{2.12}$$

where F^j is the first-order exciting force on a isolated cylinder, radius a_j in the direction of the incident wave and the upper (lower) elements refer to the force in the x- (y-) direction.

The development up to now is entirely general and Equation (2.12) with the $A^j_{\pm 1}$ found by solving (2.9) gives the forces on any of the cylinders in an arbitrary arrangement, in a given incident wave train.

We now assume the N cylinders are identical ($a_j = a$, $j = 1, \ldots, N$) and are equally-spaced around a circle of radius R. It is convenient to exploit the symmetry of the cylindrical array and choose local polar coordinates at each cylinder measured from the line joining the centre of that cylinder to the centre of the array as shown in Figure 1. It follows by elementary geometry that

$$\alpha_{jk} = \frac{\pi}{N}(k + j) + \frac{\pi}{2}\mathrm{sgn}(k - j), \tag{2.13}$$

where we have chosen cylinder j to make an angle $2\pi j/N$ with the positive x-direction ($j = 1, 2, \ldots, N$) and to have its centre at

$$x_j = R\cos(2\pi j/N), \qquad y_j = R\sin(2\pi j/N). \tag{2.14}$$

Substitution of (2.13), (2.14) in (2.9) gives

$$B^k_m + \sum_{\substack{j=1 \\ \neq k}}^{N}\sum_{n=-\infty}^{\infty} B^j_n Z^j_n H_{n-m}(\kappa R_{jk})\,\mathrm{e}^{\mathrm{i}\frac{1}{2}(n-m)\pi\,\mathrm{sgn}(k-j)}\,\mathrm{e}^{\mathrm{i}(n+m)\pi(k-j)/N}$$

$$= -I_k\,\mathrm{e}^{\mathrm{i}m(\pi/2 + 2\pi k/N - \theta_{\mathrm{inc}})}, \quad k = 1, \ldots, N, \quad -\infty < m < \infty, \tag{2.15}$$

where now

$$I_k = \mathrm{e}^{\mathrm{i}\kappa R\cos(2\pi k/N - \theta_{\mathrm{inc}})} \tag{2.16}$$

from (2.7), (2.14) and

$$R_{jk} = 2R\left|\sin\frac{\pi(k - j)}{N}\right| \tag{2.17}$$

and we have also written

$$A^k_n\exp^{2\pi kn\mathrm{i}/N} = B^k_n. \tag{2.18}$$

Note that we can obtain the same result by using local polar co-ordinates from the outset in (2.8) with A^j_n replaced by B^j_n.
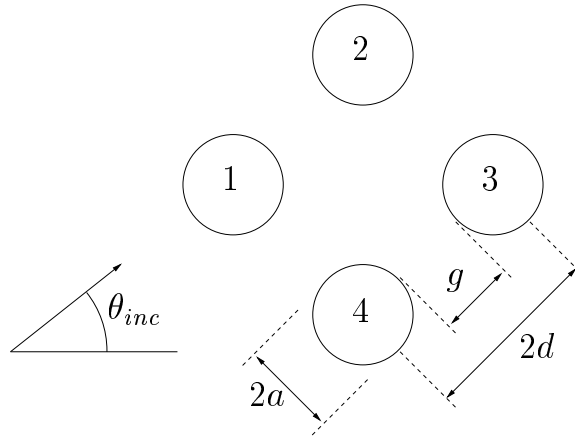
Figure 2. Arrangement, dimensions and cylinder labels for a circular arrays of four cylinders.

It is easily shown that the forces in the radial/tangential directions are

$$\frac{1}{F}\left\{\begin{array}{c} X_r^j \\ X_\theta^j \end{array}\right\} = -\frac{1}{2}\left\{\begin{array}{c} \mathrm{i} \\ 1 \end{array}\right\}\left(B_{-1}^j\left\{\begin{array}{c} - \\ + \end{array}\right\}B_1^j\right) \tag{2.19}$$

normalised with respect to the force on an isolated cylinder of radius a in the direction of the incident wave. Either (2.9) and (2.12) or (2.15) and (2.18) can be used to determine the forces on cylindrical arrays of circular cylinders and as expected they give identical results. In particular, they confirm the corrected results of Linton and Evans for the first-order exciting force on four cylinders (Linton and Evans corrigendum [9]).

3. Forces on a circular array of four identical cylinders

In this section we shall be concerned with the forces on a circular arrays of 4 cylinders arranged as shown in Figure 2. For simplicity we will only consider an incident wave progressing in the positive x-direction ($\theta_{\mathrm{inc}} = 0$) such that the cylinder labelled as one is the lead cylinder and so that the results for the forces are symmetrical. Note that this labelling is different from that used in Figure 1 and throughout the rest of the section in developing the analysis. The cylinders have diameter $2a$ with $2d$ the distance between adjacent cylinders. It is illuminating to define a gap to diameter ratio $g/2a = d/a - 1$ being the ratio of the gap between adjacent cylinders to a cylinder diameter. The circled numbers against the peaks in the curves that follow will be referred to later in the section. We derived the results by computing (2.19) using B_n calculated from (2.15).

Results for the *total* maximum force on each of four cylinders in a circular array with $\theta_{\mathrm{inc}} = 0$ against the nondimensional wavenumber κa as the ratio a/d varies are presented in Figures 3(a)–(d). In Figure 3(a), $a/d = 0.5$ as in Linton and Evans [9]. Notice the peak in the force on each cylinder at roughly the same value of $\kappa a \approx 1.66$. Figures 3(b) to (d) show the effect of bringing the cylinders closer together and it can be seen that the peaks increase markedly as a/d increases (or $g/2a$ decreases) to such an extent that for $a/d = 0.8$ ($g/2a = 0.25$) in Figure 3(d) the peak force on *all four* cylinders is some 54 times the force on an isolated cylinder. This can only be due to a near-trapped wave at the wavenumber given by
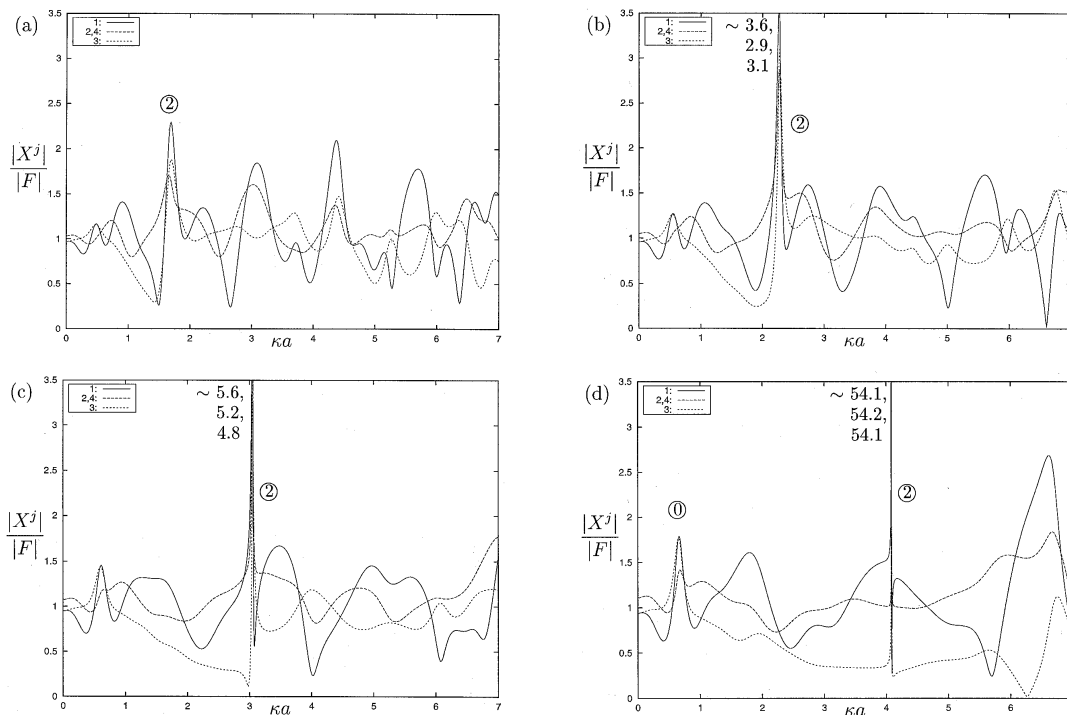
Figure 3. Resultant force on four cylinders against wavenumber, κa: $\theta_{\text{inc}} = 0$, $a/d = 0.5$ (a), 0.6 (b), 0.7 (c), 0.8 (d).

$\kappa a = 4.08482$. Results for four, five and six equally-spaced cylinders can be found in Evans and Porter [10].

We shall see later that these large forces are accompanied by large motions in the vicinity of the cylinders. In a sense this is to be expected since as the gap ratio $g/2a$ decreases the enclosed water region resembles more closely a harbour with a narrow entrance and large motions can be expected at frequencies close to the 'resonant' frequencies of the internal fluid region. This is confirmed in Figure 4 which plots, the maximum force on the lead cylinder against the gap ratio, and shows how the force increases with decreasing $g/2a$. One has to take care when numerically computing the forces for $g/2a$ smaller than 0.2, since a larger truncation parameter is needed in the infinite system of equations. That the large force is not simply a narrow entrance harbour effect can be seen from Figure 5 where the forces on four cylinders with $a/d = 0.8$ are computed when the diameter of one of the cylinders is increased by just 2%. Despite the narrowing of the gap between it and its neighbours we see by comparison with Figure 3(d) that the maximum force has reduced to less than 4.5 once the symmetry has been broken.

It is clear that the large forces and amplitudes of motion in the vicinity of the cylinders at frequencies and spacings corresponding to near-trapping are related to the near-vanishing of the determinant of the infinite system (2.15). It is also clear that this determinant is independent of the incident wave, which only appears on the right-hand side of (2.15) and that a more direct approach to near-trapping is to assume that the B_n^j are related purely through a phase factor describing the angle between cylinder k and cylinder j.
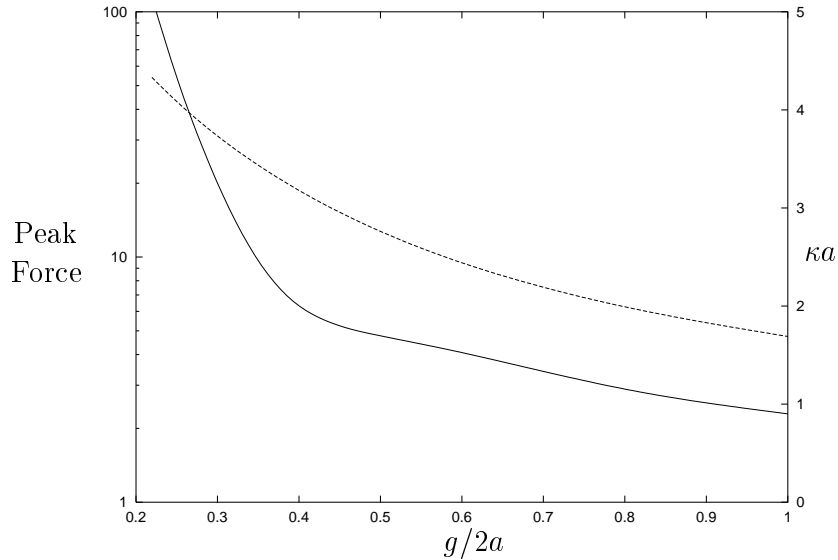
Figure 4. The variation of non-dimensional peak force (——, left scale) and wavenumber κa at which it occurs $(- - -$, right scale) on the lead cylinder in a circular array of four cylinders with $\theta_{\text{inc}} = 0$ as the gap ratio $g/2a$ varies.
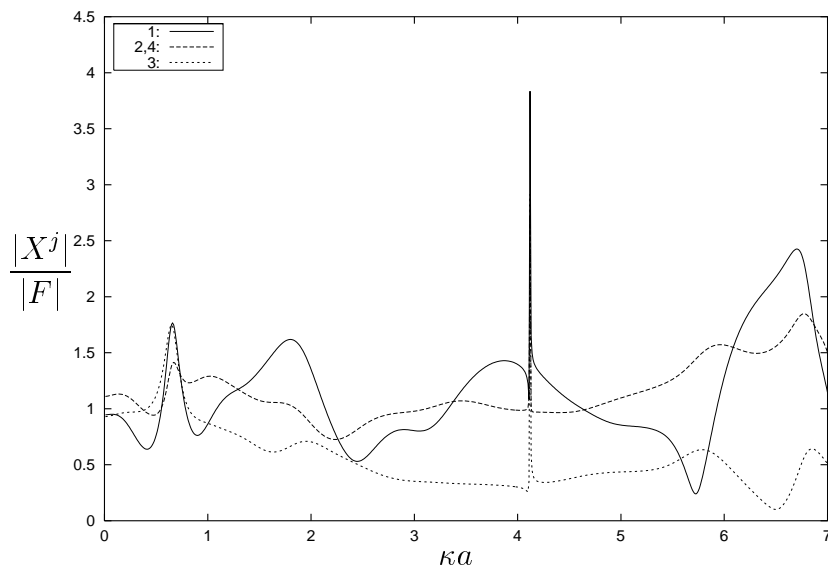

Figure 5. Resultant force on unsymmetric arrangement of four cylinders against wavenumber, κa: $\theta_{\text{inc}} = 0$, $a_1/d = 0.82$, $a_i/d = 0.8$, $i = 2, 3, 4$.

Following the approach of Maniar and Newman [6] for the linear array, we shall seek near-trapped modes directly from (2.15) by putting the RHS equal to zero and assuming a relation between the B_n^k. Thus it might be expected that, for a near-trapped mode, B_n^k would only differ from B_n^j by a phase factor reflecting the angle $2\pi(k-j)/N$ between the cylinders. More generally, whilst preserving single-valuedness, we may write

$$B_n^k = \mathrm{e}^{\mathrm{i}(k-j)2\pi p/N} B_n^j, \qquad p \text{ an integer}, \quad j, k = 1, \ldots, N, \tag{3.1}$$

whence substitution in (2.15) gives

$$B_m + \sum_{n=-\infty}^{\infty} B_n K_{mn} = 0, \tag{3.2}$$

where $B_n = B_n^0$ and the superscript zero indicates a cylinder in the 'zero-th' position on the positive x-axis. Hereafter we drop the superscript zero throughout for ease of notation. Here we have

$$K_{mn} = Z_n \sum_{\substack{j=k-1 \\ \neq 0}}^{k-N} H_{n-m}\left(2\kappa R \sin \frac{\pi |j|}{N}\right) e^{-2\pi p j i / N} e^{i\frac{1}{2}(n-m)\pi \operatorname{sgn}(j)} e^{i(m+n)\pi j / N} \tag{3.3}$$

after redefining the summation variable. This is easily seen to be independent of k when we show, in an obvious notation, that

$$K_{mn}(k) = K_{mn}(k+1), \qquad k = 1, 2, \ldots, N. \tag{3.4}$$

It follows that, in particular, we may choose $k = N$ in which case K_{mn} reduces to

$$K_{mn} = Z_n \, e^{i(n-m)\pi/2} \sum_{j=1}^{N-1} H_{n-m}\left(2\kappa R \sin \frac{\pi j}{N}\right) e^{i(m+n-2p)\pi j / N} \tag{3.5}$$

and we have reduced (2.15) to the single infinite system (3.2) with K_{mn} as above.

Now, from (3.3), we first replace the summation variable, j, by $-j$ and then substitute, without loss of generality, the value of $k = 1$ to give

$$K_{-m,-n}(p) Z_n \sum_{j=1}^{N-1} H_{n-m}\left(2\kappa R \sin \frac{\pi j}{N}\right) e^{-i\frac{1}{2}(n-m)\pi} e^{i(n+m+2p)\pi j / N} \tag{3.6}$$

in an obvious notation, but different to that used in (3.4), and comparison with (3.5) gives us

$$K_{-m,-n}(p) = (-1)^{n-m} K_{mn}(N-p) \tag{3.7}$$

whilst, it is clear from (3.5) that

$$K_{mn}(0) = K_{mn}(N). \tag{3.8}$$

It follows from using (3.7) in (3.2), that $(-1)^n B_{-n}(N-p)$ satisfies the same homogeneous equation as $B_n(p)$ and the two systems share the same determinant. This immediately gives us that the values of κd at which the determinant vanishes for a particular value of p are the same as those for $N - p$. Moreover,

$$B_n(p) = C(-1)^n B_{-n}(N-p)$$

and so

$$B_n(N-p) = C(-1)^n B_{-n}(p), \tag{3.9}$$

which implies that $C^2 = 1$ or $C = \pm 1$. In particular, choosing $p = N/2$, N even, gives

$$B_n(N/2) = \pm(-1)^n B_{-n}(N/2).$$
(3.10)

We can also use the information in (3.8) to deduce from (3.2) that $B_n(0) = C B_n(N)$, which, used in (3.9) with $p = 0$ gives

$$B_n(0) = C(-1)^n B_{-n}(0).$$
(3.11)

It remains for us to look at the radial and tangential forces due to these two modes of resonance. Thus, from (2.19) with $p = N/2$ in (3.1) to relate cylinder j to cylinder 0,

$$X_r^j(N/2) = -\tfrac{1}{2}\mathrm{i}(-1)^j(B_{-1}(N/2) - B_1(N/2)) = \begin{cases} \mathrm{i}(-1)^j B_1(N/2), & C = 1 \\ 0, & C = -1 \end{cases}$$
(3.12)

$$X_\theta^j(N/2) = -\tfrac{1}{2}(-1)^j(B_{-1}(N/2) + B_1(N/2)) = \begin{cases} 0, & C = 1 \\ -(-1)^j B_1(N/2), & C = -1. \end{cases}$$
(3.13)

In other words, the force is either radial or tangential, but never a combination of the two and switches in sign from one cylinder to the next. Likewise, with $p = 0$ (or N),

$$X_r^j(0) = -\tfrac{1}{2}\mathrm{i}(B_{-1}(0) - B_1(0)) = \begin{cases} \mathrm{i}B_1(0), & C = 1 \\ 0, & C = -1 \end{cases}$$
(3.14)

$$X_\theta^j(0) = -\tfrac{1}{2}(B_{-1}(0) + B_1(0)) = \begin{cases} 0, & C = 1 \\ -B_1(0), & C = -1 \end{cases}$$
(3.15)

giving the previous result, namely that the force can only ever be either totally radial or totally tangential, but here the sense in which the force acts is the same for all the cylinders in the array. This mode therefore corresponds to either a tangential torque on the array or a radial pull on the array. These four cases are illustrated in Figure 6. For other values of p, there does not appear to be a simple way of predicting the direction of the force on the cylinders in the array.

The four possible resonant modes summarised in Figure 6 can each be shown to possess symmetries of motion about lines joining the centre of the array to the centres of the cylinders and those from the centre passing midway between adjacent cylinders. For example, in case (a)(i) in Figure 6, using the expression for the potential close to cylinder k, we find

$$\frac{\partial \phi(r_k, 0)}{\partial \theta} = \frac{\partial}{\partial \theta}\left(\sum_{n=-\infty}^{\infty} B_n^k F_n(\kappa r_k)\mathrm{e}^{\mathrm{i}n\theta_k}\right)\Bigg|_{\theta_k=0},$$
(3.16)

where $F_n = (-1)^n F_{-n}$ is defined in (2.10). Then

$$\frac{\partial \phi(r_k, 0)}{\partial \theta} = \sum_{n=-\infty}^{\infty} \mathrm{i}n B_n^k F_n = \tfrac{1}{2}\mathrm{i}(-1)^k \sum_{n=-\infty}^{\infty} n F_n (B_n(N/2) - (-1)^n B_{-n}(N/2)),$$
(3.17)

since $p = N/2$,

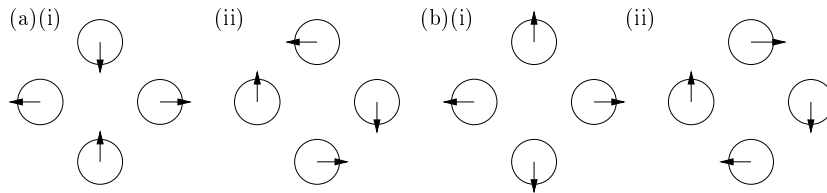$$= 0, \quad \text{for } C = 1, \text{ or case (a)(i)}$$
(3.18)

Figure 6. An illustration of the two possible forces in the resonant modes corresponding to (a) $p = N/2$, (b) $p = 0, N$.
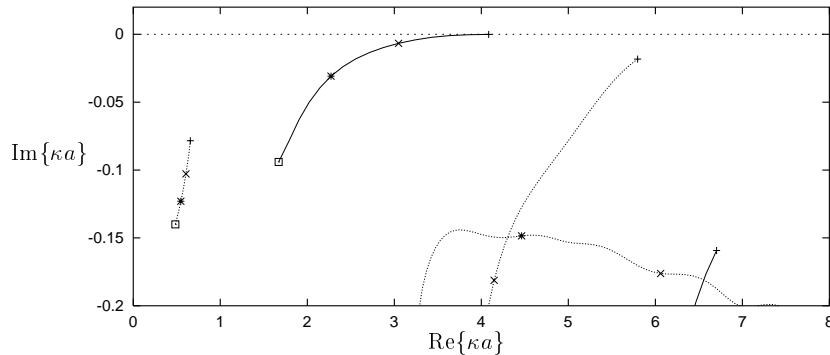

Figure 7. Location of zeros of determinant in complex wavenumber κa space for $N = 4$ cylinders as a/d varies from 0·5 to 0·8: $p = 2(\text{---})$, $p = 1(- - -)$, $p = 0(\cdots\cdots)$; $a/d = 0\cdot5(\square)$, $0\cdot6(*)$, $0\cdot7(\times)$, $0\cdot8(+)$.

and therefore there is symmetry about the lines joining the centre of the array to the centres of the cylinders. Similarly, it is trivial to show that there is antisymmetry about the lines passes midway between adjacent cylinders in this case.

It appears from our computations that all four near-trapped mode types associated with $p = 0, N/2$ and illustrated in Figure 6 exist and this can be seen more clearly by looking at the free surface plots.

3.1. FURTHER RESULTS FOR A CIRCULAR ARRAY OF FOUR IDENTICAL CYLINDERS

It is reasonable to ask whether the assumption for a near-trapped mode given in (3.1) provides all the possible resonances. Numerical experiments performed on a range of array sizes and wave parameters suggest that no others exist. In other words all resonances correspond to a value of p in the determinant system (3.2), (3.5) which has assumed (3.1) expressing only a change in phase from one cylinder to the next for the occurrence of a near trapped mode. An alternative approach would be to appeal to symmetries of the problem as was done by Gaspard and Rice [11] in their consideration of the resonances of a three disc system on which a 'soft' condition was applied.

It is the determinant system (3.2) that we turn our attention to next. Given that all resonances are accounted for by a value of p, the determinant system, in much the same way as for the infinite line of cylinders discussed earlier, provides a far more efficient way of locating the frequency at which near-trapped modes occur. Not only this, but we can also identity by, means of the value of p, the behaviour of the type of mode. The reader is reminded that choosing $N - p$ gives the same results as choosing p (this comes from equation (3.7)) and so we need only restrict ourselves to considering values of $p \leqslant [N/2]$.
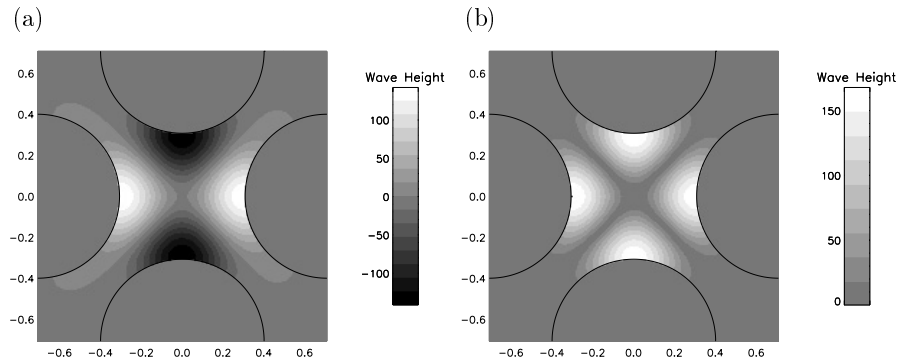
Figure 8. (a) Re $\{\phi\}$ and (b) $|\phi|$ for $N = 4, a/d = 0.8, \kappa a = 4.08482, \theta_{\text{inc}} = 0°$.
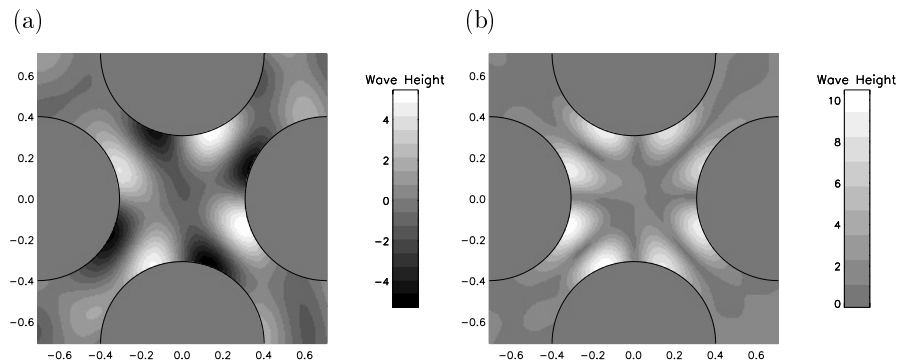

Figure 9. (a) Re $\{\phi\}$ and (b) $|\phi|$ for $N = 4, a/d = 0.8, \kappa a = 5.797, \theta_{\text{inc}} = 12\frac{1}{4}$.

For the purpose of locating the frequency at which a near-trapped mode occurs, and hence where we may expect to find large first and second order forces acting on the array, it is sufficient to scan through the nondimensional wavenumber, κa, as a real parameter and monitor the modulus of the value of the complex determinant. Then, whenever the modulus of the determinant dips close to zero, one would expect to find a resonant motion in the forcing problem. But it is perhaps more enlightening for us to seek the precise zeros of the determinant by regarding κa as a complex variable. This extra dimension adds to the computational effort in locating trapped modes, requiring the use of Newton's Method in two dimensions, but in essence is straightforward.

The zeros of the complex determinant in the cylinder array are found in the following way. For each value of p, we perform a search of the complex κa space close to the real line for a value of $a/d = 0.8$ using Newton's Method and pick out the complex values of κa corresponding to a zero of the determinant in this region. For each of these values a/d is then varied from 0.8 to 0.5 in small steps, so as to trace the path of the zero as the cylinders are separated. This provides us with the most compact way of illustrating the influence of near-trapping for any geometry consisting of N cylinders in a circular array. For example in Figure 7, it can be seen how the peak in Linton and Evans [9] is due to the real-valued κa passing 'close' to the pole in the complex plane at approximately $1.67 - 0.1i$ and, as a/d is increased to 0.8, this pole moves to within 0.001 of the real line. Furthermore, the mode corresponds to $p = 2 \, (= N/2)$. Thus, in the plots of maximum force against κa presented in Figures 3(a)–(d), the peak in the forces can be associated with the occurrence of a pole in

the complex plane close to the real axis. Clearly, as the pole moves closer to the real axis one would expect the response in the forced problem to increase. We are also able to use Figure 7 to identify the types of modes responsible for the peaks in the forces, and these are represented in Figures 3(a)–(d) by the circled values next to each of the peaks.

In order to assist our understanding of the various resonant motions due to near-trapping that have become apparent in the force plots, and whose frequencies can be predicted from the determinant system (3.2), we can also use plots of the free surface. The elevation of the free surface, $H(x, y, t) = \text{Re}\{\eta(x, y) \, e^{-i\omega t}\}$ non-dimensionalised with respect to an incident wave of unit amplitude is given by

$$\eta(x, y) = \phi(x, y). \tag{3.19}$$

In the two free surface plots presented in this section, we will use two plots: one showing $\text{Re}\{\phi\}$, the other $|\phi|$. The former of these two corresponds to the free surface elevation at a particular instant in time during the cycle, namely at $t = n\pi/\omega$, $n = 0, 1, \ldots$ (this can be seen by considering equation (2.1)), and allows us to observe the relative position of peaks and troughs. Alternatively, we could have presented plots of $\text{Im}\{\phi\}$ which corresponds to the free surface elevation at $t = (n + \frac{1}{2})\pi/\omega$, $n = 0, 1, \ldots$. Instead, we choose to plot $|\phi|$ which corresponds the maximum free surface elevation attained over a cycle. The circular array of cylinders are arranged as in Figure 2 in such a way that the distance between consecutive centres is unity ($2d = 1$), and attention is focused on the interior domain, since the motion outside the array is relatively insignificant and of little interest. Also, since it is near-trapped resonant modes that we seek, we plot the free surface due to the scattered potential only by discarding the influence of the incident wave rather than using the total potential. In the vicinity of cylinder j, say, we may use the computationally efficient method of calculating the potential given by the expression in (2.13).

Figure 8 shows the free-surface elevations $\text{Re}\{\phi\}$, $|\phi|$ at the closest real values of κa for $a/d = 0.8$. It can be seen that the maximum wave amplitude for the $a/d = 0.8$ near-trapped case is predicted at over 150 times the incident wave amplitude and is responsible for the peak in the first-order force of 54 times that on an isolated cylinder. The motion in between the cylinders resembles a floppy saddle: where there is a wave peak on one cylinder, there is a trough on a neighbouring cylinder. From Figure 7 we see that this mode is associated with a value $p = 2$ and this ties in with the prediction made by the analysis earlier for a $p = N/2$ mode where the force alternates in sign from one cylinder to the next.

The only other pole in the complex plane that comes near to the real line is the $p = 0$ mode as the cylinders are moved close together. Again, the free-surface plot in Figure 9 shows that this rather weak near-trapped mode contributes to a tangential force on the array as predicted by the theory. Note that in order to excite this mode we would need to use an incident wave that destroys the geometric symmetric of the array and we have chosen $\theta_{\text{inc}} = 12\frac{1}{4}^{\circ}$ in Figure 9 (there is nothing special about this value). However, in Figures 3(a)–(d) an incident wave with $\theta_{\text{inc}} = 0$ was used that preserved the symmetry and so no peaks corresponding to this $p = 0$ mode are observed.

For a discussion of the surface plots at near-trapping frequencies for a circular array of four, five and six identical cylinders see Evans and Porter [10].

4. Rayleigh–Bloch waves along linear arrays of cylinders

We can use similar ideas to those used in the circular arrays of the previous section to obtain solutions describing pure trapping in the case of an infinite periodic linear array of identical cylinders spaced a distance $2d$ apart along the y-axis. Such trapped waves are often termed Rayleigh–Bloch waves or edge waves and are well known from the theory of diffraction gratings. They describe localised time-periodic motions along the grating and can exist in the absence of a source of excitation such as an incident wave field. In the present case, because of symmetry of the geometry about $x = 0$, the grating is described by a periodic array of semi-circles on which a Neumann condition is satisfied protruding from a wall having either a Neumann or a Dirichlet condition imposed upon it. Rayleigh–Bloch waves along a grating with periodicity $2d$ are described by

$$\phi(x, y + 2jd) = e^{2i\beta dj}\phi(x, y), \quad j \text{ an integer} \tag{4.1}$$

and a decaying x-variation is sought such that the motion remains confined to the periodic line of cylinders.

What follows is very similar to the procedure used by Maniar and Newman [6] in showing the connection between the large forces on finite linear arrays of equally spaced identical cylinders and the trapped waves which occur in the case of an infinite periodic linear array of cylinders.

Thus we return to the general system (2.9) and apply it to an infinite line of identical cylinders spaced a distance $2d$ apart along the y-axis. Now the only effect in going from cylinder j to cylinder k is the change in the phase of the incident wave in the y-direction, $e^{2i\beta d(k-j)}$, say, where $\beta = \kappa \sin \theta_{\text{inc}}$ in accordance with (4.1). It follows from the local potential near a particular cylinder given by (2.8) that

$$A_n^k = e^{2i\beta d(k-j)} A_n^j, \quad -\infty < j, k < \infty \tag{4.2}$$

and that all A_n^k can be referred to $A_n^0 \equiv A_n$, say, where the cylinders are labelled such that cylinder j has centre $(0, 2dj)$, $-\infty < j < \infty$.

In seeking a trapped-mode solution, we discard the incident wave and seek values of κ, β satisfying the homogeneous system with $\kappa < \beta$ in general to ensure no radiation of waves for large $|x|$. By making use of (4.2), writing $j' = j - k$ and then dropping the prime, we obtain

$$A_m + \sum_{n=-\infty}^{\infty} A_n K_{mn} = 0, \quad -\infty < m < \infty, \tag{4.3}$$

where

$$K_{mn} = Z_n \sum_{\substack{j=-\infty \\ \neq 0}}^{\infty} H_{n-m}(2\kappa d|j|) \, e^{2i\beta dj} \, e^{-i\frac{1}{2}(n-m)\pi \, \text{sgn}(j)} = Z_n \mathcal{H}_{n-m}, \tag{4.4}$$

say, where

$$\mathcal{H}_{2n} = 2(-1)^n \sum_{j=1}^{\infty} H_{2n}(2\kappa dj) \cos 2\beta dj, \tag{4.5}$$

$$\mathcal{H}_{2n+1} = 2(-1)^n \sum_{j=1}^{\infty} H_{2n+1}(2\kappa dj) \sin 2\beta dj. \tag{4.6}$$

In Maniar and Newman [6], δ is used instead of βd and their cylinders are positioned on $y = 0$ rather than $x = 0$ to derive a system that is similar to (4.3), (4.4).

Clearly from (4.2) or from (4.4), we need only restrict our attention to $0 < \beta d \leqslant \pi$. Furthermore, replacing βd by $\pi - \beta d$ in (4.4), we have $K_{mn}(\pi - \beta d) = (-1)^{m-n} K_{mn}(\beta d)$ and so $(-1)^m A_m(\pi - \beta d)$ satisfies the same homogeneous equation as $A_m(\beta d)$. It follows that

$$\kappa d(\pi - \beta d) = \kappa d(\beta d)$$

and so we need only consider the range $0 \leqslant \kappa d < \beta d \leqslant \frac{1}{2}\pi$.

Note that from (4.4) $K_{-m,-n} = K_{mn}$ and so from (4.3) A_n satisfies the same homogeneous equation as A_{-n}. It follows that

$$A_n = C A_{-n} \tag{4.7}$$

for some constant C. Replacing n by $-n$ we may show that $C^2 = 1$ and substitution $n = 0$ shows that $C = 1$ provided $A_0 \neq 0$.

Twersky [12], in considering the scattering of waves by an infinite array of circular cylinders, shows how to rewrite $\mathcal{H}_n$ in a form which is rapidly convergent and his expressions for $\mathcal{H}_n$ are repeated using our notation in the Appendix. In particular, it can be seen from the Appendix that, when $0 \leqslant \kappa d < \beta d < \pi - \kappa d$, then $m_+ = -1, m_- = 0$ such that all terms in (A.1)–(A.3) containing θ_m's vanish and it follows that $\mathcal{H}_n = -\delta_{n0} + i\mathcal{Y}_n$ where $\mathcal{Y}_n$ are real. Thus, from (4.4)

$$K_{mn} = Z_n(-\delta_{mn} + i\mathcal{Y}_{n-m})$$

and substitution in (4.3) gives

$$(iA_m Z_m) + \frac{J_m'(\kappa a)}{Y_m'(\kappa a)} \sum_{n=-\infty}^{\infty} (iA_n Z_n)\mathcal{Y}_{n-m} = 0. \tag{4.8}$$

Hence, the task of finding zeros of the complex determinant in (4.3) has been reduced to finding zeros of the real determinant in (4.8) provided $0 < \kappa d < \beta d < \pi - \kappa d$

It is also possible to reduce the generally complex system (4.3) to a real system provided $\beta d = \pi$, with $\kappa d < \pi$ in a manner similar to Maniar and Newman [6]. It follows from (4.6) and the Appendix with $\beta d = \pi$, that

$$\mathcal{H}_{2n+1} = 0, \quad \text{and} \quad \mathcal{H}_{2n} = -\delta_{n0} + \frac{(-1)^n}{\kappa d} + i\mathcal{Y}_{2n}. \tag{4.9}$$

Thus, only the even values of $n - m$ occur in (4.3) and this implies that (4.3) decouples into n, m both even and n, m both odd. Now if we choose $C = 1$ in (4.7) such that $A_n = A_{-n}$ then only the odd A_n can occur. This point is justified later in this section. Then we may rewrite (4.3) as

$$A_{2m+1} + \sum_{n=-\infty}^{\infty} A_{2n+1} K_{2m+1,2n+1} = 0, \quad -\infty < m < \infty \tag{4.10}$$

and from (4.4), (4.9)

$$K_{2m+1,2n+1} = Z_{2n+1}(-\delta_{mn} + (-1)^{m-n}/\kappa d + i\mathcal{Y}_{2m-2n}).$$

Substituting this in (4.10) gives

$$(iA_{2m+1}Z_{2m+1}) + \frac{J'_{2m+1}(\kappa a)}{Y'_{2m+1}(\kappa a)} \left[\sum_{n=-\infty}^{\infty} (iA_{2n+1}Z_{2n+1})\mathcal{Y}_{2m-2n} \right.$$

$$\left. + \frac{1}{\kappa d} \sum_{n=-\infty}^{\infty} (-1)^{m-n} A_{2n+1} Z_{2n+1} \right] = 0$$

and the final sum vanishes since $Z_n = Z_{-n}$ and we have assumed $A_n = A_{-n}$. We are therefore left with a real determinant system as before. It is emphasized that this reduction to a real system only occurs on $\beta d = \pi$, $\kappa d < \pi$. Note that it is also possible for us to obtain a real system when $\beta d = \pi$ for the even A_n by choosing $C = -1$ in (4.7) to give $A_n = -A_{-n}$, although the resulting homogeneous system does not have any solutions.

For any value of βd for which (4.3) has a solution, the potential in the vicinity of cylinder j is given by (2.10), which after using (4.2) is

$$\phi^j(r_j, \theta_j) = e^{2i\beta dj} \sum_{n=-\infty}^{\infty} A_n F_n(\kappa r_j) e^{in\theta_j}. \tag{4.11}$$

Thus

$$\left. \frac{\partial \phi^j}{\partial \theta} \right|_{\theta_j = \pi/2} = e^{2i\beta dj} \sum_{n=-\infty}^{\infty} in A_n F_n(\kappa r_j) e^{in\pi/2}$$

$$= \tfrac{1}{2} i \, e^{2i\beta dj} \sum_{n=-\infty}^{\infty} n F_n(\kappa r_j) e^{in\pi/2}(A_n - A_{-n}) \tag{4.12}$$

and similarly,

$$\phi^j|_{\theta_j = \pi/2} = \tfrac{1}{2} e^{2i\beta dj} \sum_{n=-\infty}^{\infty} n F_n(\kappa r_j) e^{in\pi/2}(A_n + A_{-n}), \tag{4.13}$$

where the result $F_{-n} = (-1)^n F_n$ has been used. By virtue of (4.7) the right-hand side of either (4.12) or (4.13) vanishes and so the Rayleigh–Bloch wave is either symmetric ($A_n = A_{-n}$) or antisymmetric ($A_n = -A_{-n}$) about the line $x = 0$ for all values of βd as expected by the symmetry in the geometry.

We are therefore able to identify the type of mode by monitoring the sign of A_n/A_{-n}. The results are shown in Figure 10, where values of κd corresponding to $\beta d \leqslant \tfrac{1}{2}\pi$ are plotted for various values of a/d. The solutions described by Figure 10 satisfy Neumann conditions on each cylinder and in 10(a) they also satisfy a Neumann condition on the plane containing the centre of every cylinder, whilst in 10(b) a Dirichlet condition is satisfied on this plane. Notice that in the symmetric case, Rayleigh–Bloch waves exist for all cylinder sizes ($0 < a/d \leqslant 1$) and for all values of βd (we have concentrated on the range $\beta d \in [\tfrac{1}{4}\pi, \tfrac{1}{2}\pi]$ here; the full picture can be found in McIver *et al.* [13]). However, the situation for the antisymmetric mode
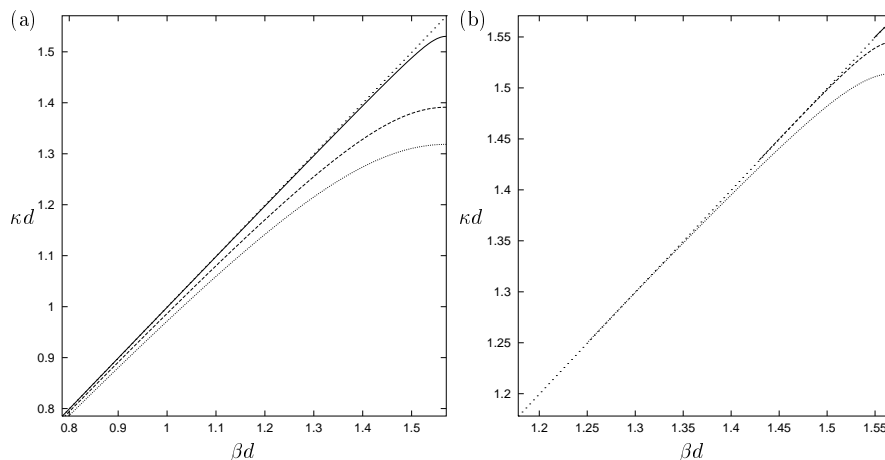
Figure 10. Rayleigh–Bloch wavenumber κd vs. βd along a cylindrical grating for various a/d. (a) The symmetric mode: $a/d = \frac{1}{4}$ (—), $\frac{1}{2}$ (- - -), $\frac{3}{4}$ ($\cdots$), (b) the antisymmetric mode: $a/d = 0\cdot85$ (—), $0\cdot9$ (- - -), $0\cdot95$ ($\cdots$).

is more complicated. Our numerical work suggests that for $a/d \lesssim 0\cdot81$, no antisymmetric mode exists for all values of βd and for values of a/d greater than $0\cdot81$, antisymmetric Rayleigh–Bloch modes only appear to exist for a limited interval $\beta d \in [\beta_0 d, \frac{1}{2}\pi]$, say.

An alternative approach to obtaining these localised surface waves has been given by McIver *et al.* [13] using appropriate periodic multipoles as in Linton and Evans [14]. This approach has the advantage of showing clearly that the modes decay to zero in a direction away from the line of cylinders, something that is not evident from the expression (4.11) derived here. Similar results for Rayleigh–Bloch modes near identical periodically-spaced cylinders of *rectangular* cross-section have been given by Evans and Fernyhough [15]. In both cases only modes symmetric about $x = 0$ are produced; the antisymmetric modes described by 10(b) are believed to be new.

In general, with time-harmonic variation re-introduced, such modes are not periodic in y, unless $2\beta d$ is a rational multiple of π, so that the modes carry energy in one direction or another along the infinite periodic array. In some cases, such as the circular cylinder array, it is possible to deduce further information from the particular form of the solution. For example, we can show that when $2\beta d$ is an integer multiple of π, the solutions reduce to standing modes and the energy remains localised near each cylinder.

Thus, it is clear from (4.6) that, whenever $2\beta d$ is an integer multiple of π, the system decouples into systems for A_{2n+1} and A_{2n}. Then from (4.11)

$$
\begin{aligned}
\phi^j(r_j, \theta_j) \pm \phi^j(r_j, -\theta_j) &= \mathrm{e}^{2\mathrm{i}\beta dj} \sum_{n=-\infty}^{\infty} (A_n F_n \, \mathrm{e}^{\mathrm{i}n\theta_j} \pm A_n F_n \, \mathrm{e}^{-\mathrm{i}n\theta_j}) \\
&= \mathrm{e}^{2\mathrm{i}\beta dj} \sum_{n=-\infty}^{\infty} F_n \, \mathrm{e}^{\mathrm{i}n\theta_j} (A_n \pm (-1)^n A_{-n}) \\
&= \mathrm{e}^{2\mathrm{i}\beta dj} \sum_{n=-\infty}^{\infty} [F_{2n} \, \mathrm{e}^{2\mathrm{i}n\theta_j} (A_{2n} \pm A_{-2n}) \\
&\quad + F_{2n+1} \, \mathrm{e}^{\mathrm{i}(2n+1)\theta_j} (A_{2n+1} \mp A_{-(2n+1)})],
\end{aligned}
\tag{4.14}
$$

We now return to our Rayleigh–Bloch waves along an infinite array and consider a value of βd close to the standing wave solution $\beta d = \frac{1}{2}\pi$, by choosing $\beta d = \frac{1}{2}\pi(1 - \varepsilon)$. Then, from (4.1)

$$\phi(x, y + 2jd) = \mathrm{e}^{\mathrm{i}j\pi(1-\varepsilon)}\phi(x, y) = \mathrm{e}^{-\mathrm{i}\pi j\varepsilon}[(-1)^{j}\phi(x, y)]. \tag{4.18}$$

The standing-wave component of the solution is contained in the square brackets, whilst the exponential term represents a modulation with one wavelength given by $j\varepsilon = 2$. Matching this modulation to the finite array, where $j = 2N$ corresponds to one wavelength gives simply that $N\varepsilon = 1$ and so

$$\beta d = \tfrac{1}{2}\pi(1 - 1/N) \tag{4.19}$$

and the corresponding wavenumber $\kappa d(\beta d)$ may be computed by means of (4.8). This value of κd provides an estimate of the frequency at which the trapped mode occurs in a finite array, and the comparison between these predicted wavenumbers and those at which there is a peak force in a finite array of N cylinders with $a/d = \frac{1}{2}$ (computed from (2.9)) is shown in Table 1. It can be seen that the agreement is excellent for $N \geqslant 25$, and even for $N = 10$ the agreement is within 1%.

More recently, J. N. Newman (personal communication) has analysed the smaller peak in the forces that occurs at a value of κd slightly lower than that for the largest peak. It was found that this value of κd corresponded to the value at which the *largest* peak occurred for an array of half the size, and that the distribution of forces along the array was now such that the cylinders a quarter and three-quarters of the way along the array experienced the largest forces, whilst the centre cylinders, in addition to the end cylinders, experienced only $O(1)$ forces. This is consistent with our analysis, since we may regard this case as either an array of N cylinders modulated by a whole wavelength, in which case we choose $N\varepsilon = 2$ from (4.18), or that of two arrays with half the number of elements joined together, each undergoing a half-wavelength modulation, when we write $\frac{1}{2}N\varepsilon = 1$. Either way results in the same value of βd and hence κd at which we expect the peak force to occur.

To add further weight to the argument connecting the Rayleigh–Bloch waves with near-trapping we compare free-surface elevations along the lines of cylinders in the two cases. Thus in Figure 11(a), we have sketched the free-surface elevation along $N = 25$ cylinders placed at $y/d = 2j$, $j = 0, 1, \ldots, 24$ when $a/d = \frac{1}{2}$ due to head seas at the near-trapping frequency. The vertical axis represents $\mathrm{Re}\{\phi(a, y/d)\}$, which is the free-surface elevation in the plane touching the outside of all cylinders at time $t = n\pi/\omega$, $n = 0, 1, \ldots$ where the amplitude of the incident wave is unity. As previously noted, the motion resembles that of a standing mode in each cell containing a cylinder along the array modulated in amplitude by a cosine-type variation. By way of comparison, in Figure 11(b) we have plotted, using the solid line, $\mathrm{Re}\{\phi(a, y/d)\}$ against y/d in the case of a Rayleigh–Bloch wave travelling along an *infinite* array. The surface-profile here is periodic in y/d with period 50 where βd is defined by (4.19) with $N = 25$, and the corresponding value of κd given in Table 1. It can be seen that the wave profile between $0 \leqslant y/d \leqslant 50$ is remarkably close to that in Figure 11(a) (overlayed with dots on Figure 11(b)) for the near-trapping case. Note that the Rayleigh–Bloch solution is homogeneous and has been scaled to match the amplitudes in Figure 11(a).

As a final remark, we notice that the earlier analysis for predicting the near-trapping frequencies is independent of the geometry and so (4.19) is applicable to a finite linear array

whilst

$$\phi^j(r_j, \theta_j) \mp \phi^{j+1}(r_{j+1}, \theta_{j+1})|_{(r_j, -\theta_j)}$$

$$= e^{2i\beta dj} \sum_{n=-\infty}^{\infty} (A_n F_n e^{in\theta_j} \mp e^{2i\beta d} A_n F_n e^{-in\theta_j})$$

$$= e^{2i\beta dj} \sum_{n=-\infty}^{\infty} F_n e^{in\theta_j} (A_n \mp e^{2i\beta d}(-1)^n A_{-n})$$

$$= e^{2i\beta dj} \sum_{n=-\infty}^{\infty} [F_{2n} e^{2in\theta_j} (A_{2n} \mp e^{2i\beta d} A_{-2n})$$

$$+ F_{2n+1} e^{i(2n+1)\theta_j} (A_{2n+1} \pm e^{2i\beta d} A_{-(2n+1)})] \tag{4.15}$$

Let us first consider the case when the mode is *symmetric* about the line joining the cylinder centres, $x = 0$. From earlier, we showed that in this case, $A_n = A_{-n}$. Let us assume that $A_{2n} \neq 0$, and $A_{2n+1} = 0$, for all n. Then, taking (4.14) with the lower sign, we render the right-hand side zero and therefore ϕ^j symmetric across $\theta_j = 0$ for all j. In other words, the solution is symmetric with respect to the planes $y = 2jd$, $\forall j$. Similar consideration of (4.15) with the appropriate sign reveals the solution is either antisymmetric (if $\beta d = \frac{1}{2}\pi$) or symmetric (if $\beta d = \pi$) across the planes $y = (2j+1)d$, $\forall j$. In both of these cases, McIver and Linton [16] have shown that no such solution exists and so we have a contradiction. We must therefore have $A_{2n} = 0$, and $A_{2n+1} \neq 0$. This argument provides the justification for choosing the system (4.10). Returning to (4.14) and (4.15) with these values, we may show that the solution is antisymmetric about the planes $y = 2jd$ and either symmetric (if $\beta d = \frac{1}{2}\pi$) or antisymmetric (if $\beta d = \pi$) about the planes $y = (2j+1)d$.

Similarly, we can analyse the case when the mode is *antisymmetric* about $x = 0$, where we have shown that $A_n = -A_{-n}$. First assume that $A_{2n} = 0$ and $A_{2n+1} \neq 0$ for all n. Then from (4.14) with the upper sign shows that ϕ^j is symmetric about $\theta_j = 0$ and hence the solution is symmetric about all planes $y = 2jd$. From (4.15) with the appropriate signs, we find that the solution is once again either antisymmetric (if $\beta d = \frac{1}{2}\pi$) or symmetric (if $\beta d = \pi$) across the planes $y = (2j+1)d$, $\forall j$. From McIver and Linton [16], such conditions cannot give rise to trapped modes. Thus, we must have $A_{2n} \neq 0$ and $A_{2n+1} = 0$ in the case of a mode antisymmetric about $x = 0$ though $A_0 = 0$ is also required so as not to contradict (4.7). Consequently, the solution is antisymmetric about the planes $y = 2jd$ and either symmetric (if $\beta d = \frac{1}{2}\pi$) or antisymmetric (if $\beta d = \pi$) about the planes $y = (2j+1)d$ as in the previous case.

Thus, in each case the motion reduces to a standing wave mode in each interval $y \in [(2j - 1)d, (2j+1)d]$. We can replace the entire configuration using images by a single cylinder on the mid-plane, $y = 0$, of a channel $|y| < d$, $-\infty < x < \infty$ for which

$$\phi = 0, \quad \text{on } y = 0, |x| > a$$

and *either* $\quad \phi_y = 0, \quad \text{on } y = |d|, \quad (\beta d = \frac{1}{2}\pi), \tag{4.16}$

$\quad \text{or} \quad \phi = 0, \quad \text{on } y = |d|, \quad (\beta d = \pi). \tag{4.17}$

When $\phi_x = 0$ on $x = 0$ and (4.16) is chosen gives precisely the condition for trapped modes discovered by Callan *et al.* [7], whilst (4.17) completes the conditions satisfied by the Dirichlet

Table 1. Table showing the values of κd at which large forces occur in a linear array of N cylinders, $a/d = \frac{1}{2}$ and the wavenumbers predicted using Rayleigh–Bloch theory.

N (no. of cylinders)	$\beta d = \frac{1}{2}\pi(1 - 1/N)$	$\kappa d(\beta d)$	κd (peak force)
100	1·5550	1·3907	1·3907
50	1·5394	1·3889	1·3889
25	1·5080	1·3818	1·3820
20	1·4923	1·3767	1·3775
15	1·4661	1·3659	1·3680
10	1·4137	1·3376	1·3470

trapped modes described by Maniar and Newman [6]. The antisymmetric modes, where $\phi = 0$ on $x = 0$, are described briefly in Evans and Porter [17] in the note added in proof. We return to these trapped modes in Section 5.

4.1. APPLICATION OF RAYLEIGH–BLOCH THEORY TO NEAR-TRAPPING BY FINITE LINEAR ARRAYS OF CYLINDERS

In the final part of this section we make a connection between Rayleigh–Bloch waves and the near-trapping of waves by large but *finite* linear periodic arrays of vertical cylinders as described in Maniar and Newman [6]. They showed that when an incident wave of a certain frequency interacts with a large array of evenly spaced cylinders in a line, large forces are experienced by the cylinders near the centre of the array corresponding to large near-resonant motions of the surrounding fluid. The frequencies at which these large responses occurred were found to be close to those trapped mode frequencies for a single cylinder between two walls having Neumann or Dirichlet conditions imposed upon them described at the end of the previous section. The former case is obtained by taking $\beta d = \frac{1}{2}\pi$, and it is possible to make a stronger connection between near-trapping by finite arrays and trapped modes about infinite arrays of cylinders by considering the Rayleigh–Bloch solutions for general βd.

In what follows we are motivated by Figure 2(b) in Maniar and Newman [2] in which the distribution of forces along a finite array of 100 cylinders at the 'near-trapping' frequency is plotted as a function of distance along the array and shows that the maximum force (of approximately 34 times the isolated cylinder force) is experienced by the centre cylinder, with the forces falling off to $O(1)$ at the two ends of the array.

Thus, the wave motion at this near-trapping frequency would appear to be a near-standing mode in each cell containing a cylinder, but modulated in amplitude along the array with one wavelength equal to twice the length of the array. This is confirmed by Figure 11(a) which shows the free-surface elevation in the plane touching the outside of all 25 cylinders placed at $y/d = 2j$, $j = 0, \ldots, 24$ in head seas at the near-trapping frequency. Clearly, in each cell $y/d \in [2j - 1, 2j + 1]$ containing a cylinder, the wave appears to be of the standing-mode type modulated in amplitude by half a cosine wave along the array.
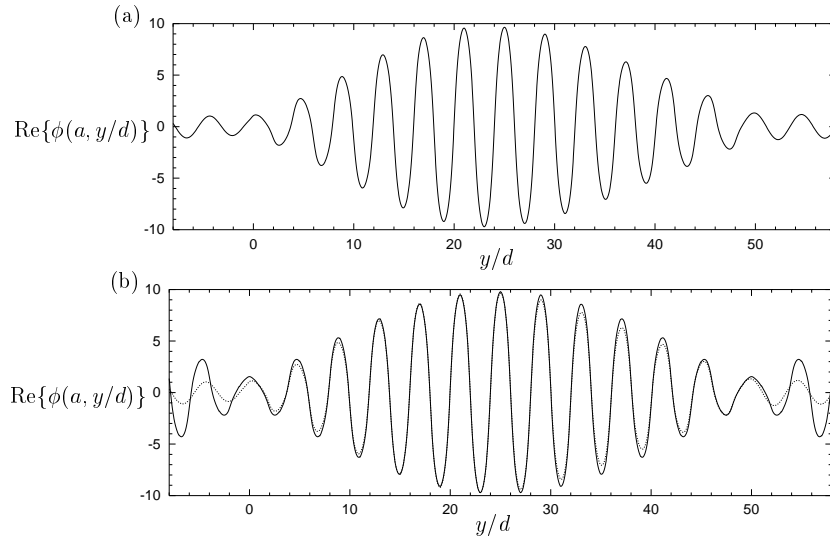
Figure 11. (a) The free-surface elevation along $N = 25$ cylinders at the near-trapping frequency ($a/d = \frac{1}{2}$), and (b) overlayed ($\cdots$) on the Rayleigh–Bloch surface profile (—) along a corresponding infinite array with βd given by (4.19).

consisting of elements of any cylinder cross section for which Rayleigh–Bloch waves exist in the corresponding infinite array. More work is currently being done here.

5. Trapped waves in channels

In this section we describe the method of Callan *et al.* (1991) for predicting trapped modes near a circular cylinder in a channel, but allow for the possibility of obtaining further solutions at wavenumbers embedded in the continuous spectrum prompted by the numerical work of the previous section. Two types of modes will be sought: Neumann(N) modes for which the normal derivative of the velocity potential vanishes on the channel walls, and Dirichlet(D) modes for which the solution itself vanishes on the walls. A further sub-division is made into modes which are symmetric about a plane through the cylinder normal to the channel walls, NS or DS modes, and modes which are antisymmetric about this plane, designated NA or DA modes.

The velocity potential Φ is expressed by (2.1) where, for the NS modes, $\phi(x, y)$ satisfies

$$(\nabla^2 + \kappa^2)\phi = 0, \quad \text{in } r > a, \quad |y| < d, \quad r = (x^2 + y^2)^{1/2}, \tag{5.1}$$

$$\phi_y = 0, \quad |y| = d, \quad -\infty < x < \infty, \tag{5.2}$$

$$\phi_r = 0, \quad r = a, \tag{5.3}$$

$$\phi = 0, \quad y = 0, \quad |x| \geqslant a, \tag{5.4}$$

$$\phi \to 0, \quad |x| \to \infty, \quad |y| \leqslant d, \tag{5.5}$$

$$\phi_x = 0 \quad x = 0, \quad |y| > a, \tag{5.6}$$

and κ is given by (2.2). We seek possible solutions of the above equations for values of κ satisfying

$$0 < \kappa < 3\pi/2d. \tag{5.7}$$

In seeking DS trapped modes we replace (5.2) by

$$\phi = 0, \quad |y| = d, \qquad -\infty < x < \infty \tag{5.8}$$

and look for possible solutions for values of κ satisfying

$$0 < \kappa < 2\pi/d. \tag{5.9}$$

For NA or DA modes, we replace (5.6) by $\phi = 0$, $x = 0$, $|y| > a$. We focus attention on possible NS modes and indicate at the end the minor the changes needed in considering the other possible mode types.

It is sufficient to consider $0 \leqslant y \leqslant d$ and choose functions odd in y in order to satisfy (5.4).

The fundamental singular solution $iH_{2n+1}^{(1)}(\kappa r) \sin(2n+1)\theta$ where $r \cos \theta = x$, $r \sin \theta = y$, satisfying (5.1), (5.4) and (5.6) may be modified by including an integral term, in order to satisfy (5.2). The resulting multipole turns out to be purely real, and to satisfy (5.5) provided that $\kappa < \pi/2d$. If now $0 < \kappa < 3\pi/2d$, the modifying integral term is now indeterminate, having a pole on the real path of integration. It is normal in such a case, on physical grounds, to choose a path which passes below the pole so that the now complex-valued integral behaves like a wave travelling outwards at large distances. If we do this, the total multipole potential is no longer real and the resulting infinite system is complex and we would be left with the task of showing that the determinant had a real zero and that the corresponding expansion coefficients were such as to produce no waves at infinity. Instead, we proceed differently. The modifying integral term can also be made determinate if we interpret it as a principal-value integral. This has the advantage that it remains real, whilst its behaviour at large distances is now a standing wave. Thus, the resulting infinite system is also real and we have a simpler task of computing any real zeros of the real determinant which simultaneously produce a combination of standing waves which vanish at large distances.

We find (see Callan *et al.* (1991)) that we have for the multipoles the expressions

$$
\begin{aligned}
\psi_{2n+1}(r, \theta) = \ & Y_{2n+1} \sin(2n + 1)\theta \\
& - \frac{2(-1)^n}{\pi} \int_0^\infty \frac{e^{-\gamma d}}{\cosh \gamma d} \sinh \gamma y \cos(\kappa x \cosh v) \sinh(2n + 1)v \, dv \\
& - \frac{2}{\pi} \int_0^{\frac{1}{2}\pi} \tan \beta d \sin \beta y \cos(\kappa x \sin u) \cos(2n + 1)u \, du,
\end{aligned}
\tag{5.10}
$$

where $\gamma = \kappa \sinh v$, $\beta = \kappa \cos u$, or equivalently

$$
\begin{aligned}
\psi_{2n+1}(r, \theta) = \ & -\frac{2(-1)^n}{\pi} \int_0^\infty \frac{\cosh \gamma (d - y)}{\cosh \gamma d} \sinh \gamma y \cos(\kappa x \cosh v) \sinh(2n + 1)v \, dv \\
& - \frac{2}{\pi} \int_0^{\frac{1}{2}\pi} \frac{\cos \beta (d - y)}{\cos \beta d} \cos(\kappa x \sin u) \cos(2n + 1)u \, du.
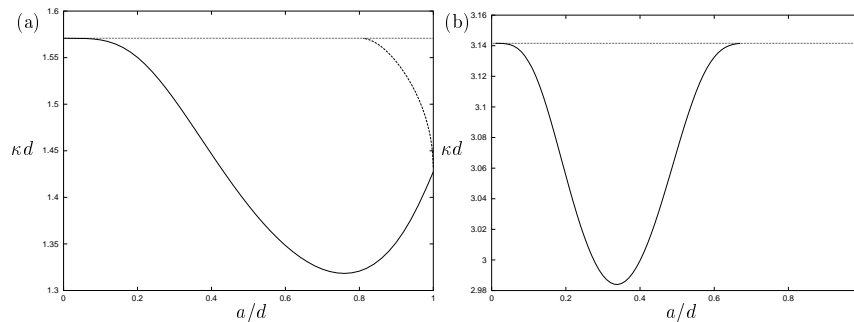\end{aligned}
\tag{5.11}
$$

Figure 12. (a) The Neumann trapped mode wavenumbers $0 < \kappa d < \frac{1}{2}\pi$ vs. cylinder size a/d: (—) symmetric mode (NS), (- - -) antisymmetric mode (NA). (b) The Dirichlet (DS) trapped mode wavenumbers $0 < \kappa d < \pi$ vs. a/d.
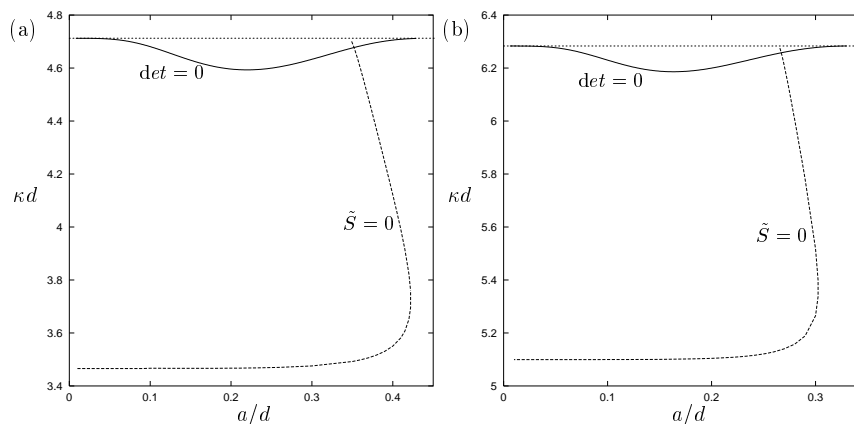

Figure 13. Curves showing zeros of determinant and of $\tilde{S}$ for the (a) Neumann and (b) Dirichlet modes as functions of κd and a/d.

It is clear from (5.10) that (5.4) is satisfied and from (5.11) that (5.2) is satisfied. Note the single principal value in the integrals if $\pi/2d < \kappa < 3\pi/2d$ and which is not needed if $0 < \kappa d < \pi/2d$. The behaviour of $\psi_{2n+1}(r, \theta)$ for large $|x|$ can be determined from (5.11) as follows. The first integral vanishes for large $|x|$ by the Riemann–Lebesgue lemma and we can write the second as

$$I = -\frac{2}{\pi} \operatorname{Re} \int_0^{\frac{1}{2}\pi} \frac{\cos \beta(d-y)}{\cos \beta d} e^{i\kappa x \sin u} \cos(2n+1)u \, du. \tag{5.12}$$

Now $\cos \beta d = 0$ when $\cos u = (2n+1)\pi/2\kappa d$, $n = 0, \pm 1, \ldots$. But $\frac{1}{3} < \pi/2\kappa d < 1$ if $\pi/2d < \kappa < 3\pi/2d$ so that there is just one root, $u = u_0$, say, when $n = 0$, on the path of integration. Thus

$$\beta_0 = \kappa \cos u_0 = \pi/2d.$$

If we now close the integral for I by a small semi-circle about $u = u_0$ in the upper u-plane, the resulting complex integral is easily seen, by deforming the path slightly upwards, to vanish at

$x \to \infty$, leaving a term arising from the integral around the small circle. Thus, evaluating the (half) residue, we have

$$I \sim -\frac{2}{\pi} \mathrm{Re}\,\pi i \frac{\cos \beta_0 (d - y) \mathrm{e}^{\mathrm{i}\kappa x \sin u_0}}{\kappa d \sin \beta_0 d \sin u_0} \cos(2n + 1)u_0, \quad \text{as } x \to \infty. \tag{5.13}$$

For $x \to -\infty$, the integral path is closed by a semi-circle in the lower half-plane with the final result, since I is even in x,

$$\psi_{2n+1}(r, \theta) \sim \frac{2 \sin \beta_0 y \sin(\kappa |x| \sin u_0)}{\kappa d \sin u_0} \cos(2n + 1)u_0, \quad |x| \to \infty. \tag{5.14}$$

If $0 < \kappa < \pi/2d$ then $\psi_{2n+1}(r, \theta) \to 0$ as $|x| \to \infty$. We now seek a trapped mode in the form

$$\phi(r, \theta) = \sum_{n=0}^{\infty} \kappa^{-1} a_n (Y'_{2n+1}(\kappa a))^{-1} \psi_{2n+1}(r, \theta) \tag{5.15}$$

and application of the condition (5.3) yields

$$a_m + \sum_{n=0}^{\infty} B_{mn} a_n = 0, \quad m = 0, 1, 2, \dots \tag{5.16}$$

where $B_{mn} = A_{mn} J'_{2m+1}(\kappa a)/Y'_{2n+1}(\kappa a)$. Here

$$A_{mn} = -\frac{4}{\pi}(-1)^{m+n} \int_0^{\infty} \frac{\mathrm{e}^{-\gamma d}}{\cosh \gamma d} \sinh(2n + 1)v \, \sinh(2m + 1)v \, \mathrm{d}v$$

$$-\frac{4}{\pi} \int_0^{\frac{1}{2}\pi} \tan \beta d \cos(2n + 1)u \cos(2m + 1)u \, \mathrm{d}u, \tag{5.17}$$

where the principal value is not necessary if $0 < \kappa < \pi/2d$. Also, from (5.14), (5.15) if $\pi/2d < \kappa < 3\pi/2d$ we require

$$S = \sum_{n=0}^{\infty} \frac{a_n \cos(2n + 1)u_0}{Y'_{2n+1}(\kappa a)} = 0 \tag{5.18}$$

ensuring that

$$\phi(r, \theta) \sim \frac{2S \sin \beta_0 y}{\kappa^2 d \sin u_0} \sin(\kappa |x| \sin u_0), \quad |x| \to \infty \tag{5.19}$$

satisfies condition (5.4).

5.1. Results

The computation of the real zeros of the real determinant of the system (5.16) is straightforward for $0 < \kappa d < \frac{1}{2}\pi$ when the principal value interpretation in (5.17) is not needed and $S = 0$. It is found that a unique value of trapped mode wavenumber κd exists for each value
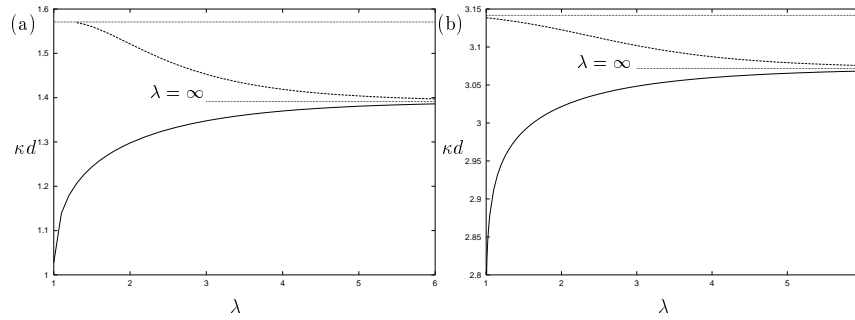
Figure 14. Variation of (a) Neumann and (b) Dirichlet trapped mode frequencies for two cylinders, both $\mu = \frac{1}{2}$ as the spacing parameter, λ, varies. Symmetric modes (—), antisymmetric modes (- - -).
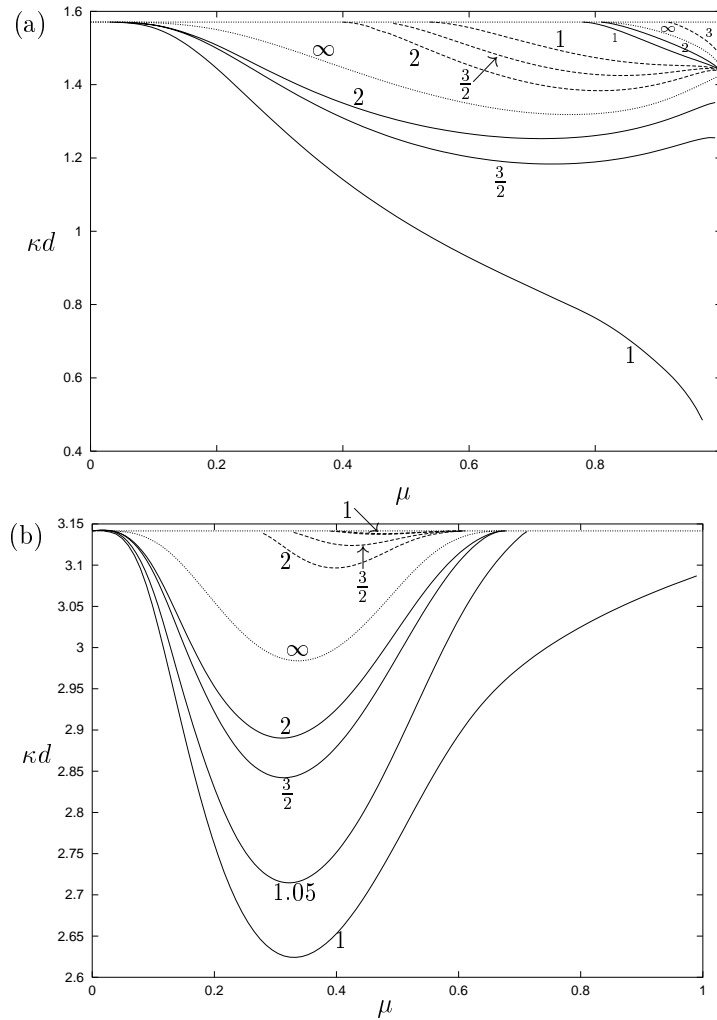

Figure 15. Variation of (a) Neumann and (b) Dirichlet trapped-mode frequencies as μ varies in the case of two cylinders for different values of the spacing parameter λ (shown against the curves). Symmetric modes (—), antisymmetric modes (- - -).

of a/d. This is illustrated in Figure 12(a) by the solid curve and are just those results to be found in Callan *et al.* [7]. For $\frac{1}{2}\pi < \kappa d < \frac{3}{2}\pi$ we need to consider the principal-value integral in (5.17) in computing the values of κd for which the determinant of (5.16) vanishes as a function of a/d. Just as for values of $\kappa d < \pi/2$, there is a unique value of κd for each a/d, and a single curve of κd versus a/d can be drawn. At each point on this curve a non-trivial vector $\mathbf{a} = \{a_0, a_1, \ldots\}$ is defined allowing S to be computed from (5.18). Then any points on the curve of vanishing determinant for which S *also* vanishes corresponds to a trapped mode. This provides a method for determining the values of κd and a/d for which trapped modes occur. Instead, however, we choose to proceed slightly differently. The advantage of the method below will become clear later.

Let the eigenvalues of the matrix $\delta_{mn} + B_{mn}$, $m, n = 0, 1, 2, \ldots$ in the system (5.16) be $\{\lambda_r\}$, each λ_r having a corresponding eigenvector $\mathbf{e}^r = \{e_0^r, e_1^r, \ldots\}$. Let $\lambda_m = \min_r\{|\lambda_r|\}$ and define

$$\tilde{S} = \sum_{n=0}^{\infty} \frac{e_n^m \cos(2n+1)u_0}{Y_{2n+1}'(\kappa a)} \tag{5.20}$$

Unlike S in (5.18), $\tilde{S}$ is defined over all parameters κd and a/d and not just on the curve of vanishing determinant. However, the values of S and $\tilde{S}$ do coincide on the curve of det $= 0$ where $\lambda_m = 0$, and the corresponding eigenvector $\mathbf{e}^m$ is equal to $\mathbf{a}$. Thus, if in addition to the curve det $= 0$, the curve $\tilde{S} = 0$ is also sketched, then any points of intersection of these two curves correspond to a trapped mode. The advantage of this method is that a trapped mode is clearly seen to correspond to the crossing of two lines and that the values of κd and a/d for which a trapped mode occurs can easily be read off the graph. Moreover, as series are computed numerically by truncation and curves are not exact, it is more convincing for us to have two independently computed curves intersecting rather than using the information from an 'approximate' curve in a further condition that must also be satisfied. For values of $\kappa d \in (\pi/2, 3\pi/2)$ we plot points where $\tilde{S}$, given by (5.20) vanishes. Again this provides a unique curve of κd against a/d. The curves are shown in Figure 13(a), where it can be seen that there is just one intersection indicating a trapped mode.

Increasingly refined calculations give the values at which this embedded Neumann trapped mode occurs as

$$\kappa d = 4{\cdot}677467 = 1{\cdot}488884\pi \quad \text{and} \quad a/d = 0{\cdot}3520905.$$

The procedure for determining the embedded DS trapped mode follows that outlined above for the Neumann modes with only minor changes arising from the replacement of (5.2) by (5.8) in the governing equations. Fundamentally this affects the form of the multipoles defined in the Neumann case by (5.10). Thus, the changes for the Dirichlet case involve the replacement of $\cosh \gamma d$ by $\sinh \gamma d$ in the denominator of the first integral in (5.10) and of $\tan \beta d$ by $-\cot \beta d$ in the second. Working through with these altered expressions still gives the two Equations (5.16) and (5.18) (and therefore (5.20)), but in (5.17), $\cosh \gamma d$ is replaced with $-\sinh \gamma d$ and $\tan \beta d$ is replaced with $-\cot \beta d$. Note also that now the principal value occurs at the value $u = u_0$ where $\beta_0 = \kappa \cos u_0 = \pi/d$.

Results for the Dirichlet mode are also shown in Figure 13(b) as the intersection of two curves. Precise values for this new embedded modes are

$$\kappa d = 6{\cdot}257636 = 1{\cdot}991867\pi \quad \text{and} \quad a/d = 0{\cdot}2670474.$$

For the Dirichlet mode when $0 < \kappa d < \pi$ the principal value is not required and $S = 0$ and the computation of the zeros of the determinant show that there exists a unique Dirichlet trapped-mode wavenumber κd for each value of $a/d \lesssim 0 \cdot 6788$. A curve showing the variation of κd against a/d in this case is given in Figure 12(b).

Possible NA modes (Neumann conditions on the channel walls and an antisymmetric about the line through the centre of the cylinder perpendicular to the channel walls) can be constructed in a manner similar to before, starting with a modification of the Callan *et al.* [7] multipoles to enforce the antisymmetry condition, the resulting homogeneous system again being (5.16), but with $B_{mn} = A_{mn} J'_{2m}(\kappa a)/Y'_{2n}(\kappa a)$ and A_{mn} replaced by

$$A_{mn} = -\frac{4}{\pi}(-1)^{m+n} \int_0^\infty \frac{e^{-\gamma d}}{\cosh \gamma d} \sinh 2mv \sinh 2nv \, dv$$

$$-\frac{4}{\pi} \int_0^{\frac{1}{2}\pi} \tan \beta d \sin 2mu \sin 2nu \, du \tag{5.21}$$

where $\gamma = \kappa \sinh v$, $\beta = \kappa \cos u$ as before. If $0 < \kappa d < \frac{1}{2}\pi$, a real zero of the infinite determinant of (5.16) exists for all values of $a/d \gtrsim 0 \cdot 81$. The NA trapped modes are shown in Figure 12(a) by the dashed curve.

Computations suggest that no DA trapped modes exist for $0 < \kappa d < 2\pi$ and the same is true for NA modes if $\frac{1}{2}\pi < \kappa d < \frac{3}{2}\pi$. Further details can be found in Evans and Porter [18]. See also Evans and Porter [17].

6. Trapped modes about multiple cylinders in a channel

In this section, we describe the results of extending the theory of Callan *et al.* [7] to multiple cylinders centred on the centre-plane of a channel and determine the corresponding Neumann and Dirichlet trapped modes. We omit the details which can be found in Evans and Porter [17]. In brief, for each cylinder a general multipole expansion satisfying all conditions except on the cylinders themselves can be constructed and Grafs addition theorem for Bessel functions used in applying the Neumann condition on each cylinder. This produces a homogeneous real infinite system of equations for the Fourier coefficients associated with each cylinder.

The number of possible configurations of cylinders we could consider is of course limitless, but we shall concentrate here on the case of two identical cylinders because of its connection with *finite* double arrays of cylinders which occur in offshore floating structures as discussed in the Introduction. The nondimensional trapped-mode wavenumber κd is in this case a function of two dimensionless parameters μ and λ describing the size and spacing of the centres of the cylinders. We choose $\mu = a/d$ and let the centres of the cylinders be located at $(\pm\lambda a, 0)$, so that λ is a spacing parameter being the ratio of cylinder separation to cylinder diameter. When $\lambda = 1$, the cylinders are touching and, as $\lambda \to \infty$, we would expect results for the trapped modes to approach the single cylinder results as the interaction between them diminishes. In fact, since the trapped modes are a localised phenomenon, we might expect the single cylinder results to be approached for relatively small values of λ. This proves to be the case as Figure 14 illustrates. Here, Neumann and Dirichlet trapped mode wavenumbers κd obtained by computing the real zeros of the determinant in the homogeneous real infinite system for the Fourier coefficients are plotted against μ for different λ. Also shown is the unique wavenumber for both the Neumann and Dirichlet trapped modes for an isolated cylinder which we label
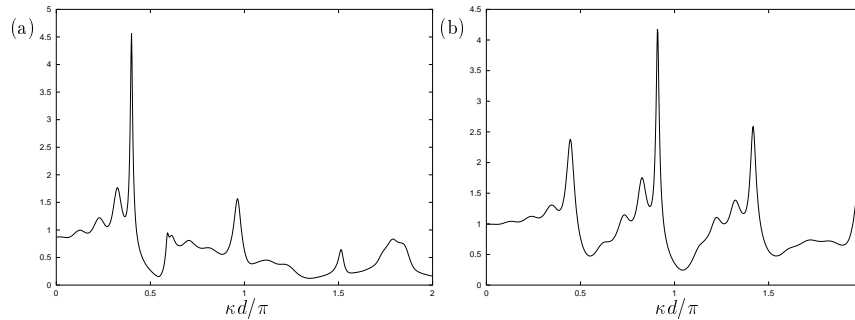
Figure 16. Maximum exciting force against non-dimensional wavenumber κd in the case of head seas interacting with a double array of 2×9 cylinders all of radius a. The two rows are $4a$ apart and in each row the centres are $2d$ apart. (a) $a/d = \frac{1}{2}$, (b) $a/d = \frac{1}{4}$.

$\lambda = \infty$. We consider the Neumann modes first, all of whose wavenumbers satisfy $\kappa d < \pi/2$. The solid curves are symmetric Neumann trapped modes whilst the dashed curves above the $\lambda = \infty$ curve are all antisymmetric Neumann trapped modes, the symmetries measured across the mid-plane between the two cylinders. We can draw the following conclusions about the Neumann modes from Figure 14.

For sufficiently large μ and λ there exist four Neumann trapped modes, two symmetric and two antisymmetric about the mid-plane between the two cylinders. As λ increases one of each type converges to the unique value of the Neumann mode NS, for a single cylinder for that μ, whilst the other pair converge to the Neumann mode NA for a single cylinder. See the beginning of Section 5 for the definition of these abbreviations. These single cylinders results are labelled by $\lambda = \infty$ in Figure 15(a). However, for fixed λ as μ decreases, eventually only a single symmetric curve remains. The behaviour is made clearer in Figure 15(a) which, for a fixed value of $\mu = 0.9$, shows how the trapped mode wavenumbers vary with spacing parameter, λ. The Dirichlet modes are shown in Figure 15(b). Whilst a maximum of only two modes can exist for the Dirichlet modes, the general behaviour of the Dirichlet modes is more complicated than the Neumann modes. Maniar and Newman [6] showed that, for an isolated cylinder, Dirichlet modes only exist for $0 < \mu \lesssim 0.6788$ and this is confirmed in Figure 15(b) by the $\lambda = \infty$ curve (also illustrated in Figure 12). The presence of a second identical cylinder widens the range of μ for which (symmetric) Dirichlet modes exist and this range increases slowly as the gap between the cylinders is reduced. Thus, even for $\lambda = 1.05$ when the fluid gap is only 5% of a cylinder diameter, the range of existence has only increased up to $\mu \approx 0.772$. However, computations right down to $\lambda = 1$ corresponding to touching, suggest that a symmetric Dirichlet mode exists for *all* $\mu \in (0, 1)$. Note that at $\lambda = \mu = 1$ each of the two exterior fluid regions is the same as the region exterior to a single cylinder with $\mu = 1$ for which Figure 12 shows there is no solution. One explanation is that in this limit the trapped-mode frequency coincides with a sloshing frequency in the two identical bounded cusped interior regions. In addition to this complicated behaviour for $\lambda \approx 1$, the antisymmetric Dirichlet modes, just as for the Neumann modes, also manifest a cut-off below certain values of μ for each λ so that the overall picture is one of existence of antisymmetric Dirichlet modes in intervals of μ for given λ which increase in length with increasing λ up to $0 < \mu \lesssim 0.6788$ and the existence of symmetric Dirichlet modes for all μ for λ sufficiently close to unity, or a cut-off above some value μ_0 with $0.6788 \lesssim \mu_0 \leqslant 1$ for each λ.

It is possible to remove the channel walls and regard both types of trapped modes as oscillations between adjacent pairs of cylinders in a doubly-infinite row, the Neumann modes having an antinode at each mid-plane between pairs of cylinders and the Dirichlet modes a node. Following the discussion of Maniar and Newman [6] that a *finite* single row containing many cylinders could experience large forces and free-surface motions at frequencies close to the Neumann and Dirichlet trapped modes for a single cylinder in a channel, or its equivalent *infinite* row of cylinders, we should expect that the peaks in Figures 16(a) and 16(b) which give the maximum in-line exciting force on the middle pair of cylinders in a double row of 2×9 cylinders due to head seas to be close to the corresponding symmetric trapped modes. In Figures 16(a), 16(b) the distance between two cylinders in a pair is $4a$ so that in both figures the corresponding doubly-infinite row requires $\lambda = 2$. It is clear from Figure 14 at $\lambda = 2$ that this is indeed the case. Thus, the computed values of the symmetric Neumann and Dirichlet trapped-mode wavenumbers for $\mu = \frac{1}{2}$ are $\kappa d = 1 \cdot 29771$ and $\kappa d = 3 \cdot 02157$, respectively, compared to the peaks at $1 \cdot 256$ and $3 \cdot 024$ in Figure 16(a), whilst for $\mu = \frac{1}{4}$ the trapped modes at $\kappa d = 1 \cdot 46567$ and $2 \cdot 90894$ compare to the peaks at $1 \cdot 400$ and $2 \cdot 856$ respectively in Figure 16(b). The other peaks in Figures 16(a),(b) are believed to correspond to nearly-trapped waves. Notice how the dominant mode in Figure 16(a) when $\mu = \frac{1}{2}$ is a symmetric Neumann mode, whereas in Figure 16(b) when $\mu = \frac{1}{4}$ the symmetric Dirichlet mode dominates. The same behaviour was found by Maniar and Newman [6, Figure 1] in considering a single row of cylinders.

Because Figure 16 describes the exciting forces in head seas, it shows no evidence of the antisymmetric Neumann trapped modes at $\mu = \frac{1}{2}$ shown in Figure 14(b) for $\lambda = 2$. Computations for a double row of nine cylinders in obliquely-incident waves having an antisymmetric component again provide little indication of the antisymmetric mode whilst the peak for the symmetric mode is reduced. It appears to be difficult for us to generate a significant peak close to the antisymmetric trapped modes in a finite double row by using a physically realistic wave train. However, it proves possible, using equal and opposite obliquely-incident waves which are antisymmetric about the mid-line between the two rows of cylinders, for us to create a similar amplification to that shown in Figure 16 in the wave forces on the middle cylinders close to the antisymmetric Neumann mode for $\mu = \frac{1}{2}$.

If we consider two unequal cylinders, the two trapping-mode curves against λ approach corresponding values for each cylinder in isolation as λ increases. Similar considerations apply as the number of cylinders is increased. Further examples are provided in Evans and Porter [17].

7. Conclusion

A variety of problems concerned with the trapping or near-trapping of waves by arrays of bottom-mounted identical vertical cylinders has been considered, reflecting the latest results in this rapidly-developing area. The connection between the possibility of large exciting forces and corresponding trapped-mode configurations will ensure that the fascinating subject of trapped modes will continue to attract interest for practical as well as theoretical reasons.

Appendix. The Schlömilch series

According to Twersky (1961), for $n \geqslant 1$,

$$
\mathscr{H}_{2n} = \frac{(-1)^n}{\kappa d} \sum_{m=-m_-}^{m_+} \frac{\cos 2n\theta_m}{\cos \theta_m} - \frac{\mathrm{i}(-1)^n}{\kappa d} \left(\sum_{m=0}^{m_+} - \sum_{m=-1}^{-m_-} \right) \frac{\sin 2n\theta_m}{\sin \theta_m} + \frac{\mathrm{i}(-1)^n}{n\pi}
$$

$$
+ \frac{\mathrm{i}}{\pi} \sum_{m=1}^{n} \frac{(-1)^{m-n}(n+m-1)! B_{2m}(\beta d/\pi)}{(2m)!(n-m)!(\kappa d/2\pi)^{2m}}
$$

$$
- \frac{\mathrm{i}}{\kappa d} \left[\sum_{m=m_++1}^{\infty} \frac{\mathrm{e}^{-2nl_m^+}}{\sinh l_m^+} + \sum_{m=m_-+1}^{\infty} \frac{\mathrm{e}^{-2nl_m^-}}{\sinh l_m^-} \right] \tag{A.1}
$$

and for $n \geqslant 0$,

$$
\mathscr{H}_{2n+1} = -\frac{\mathrm{i}(-1)^n}{\kappa d} \sum_{m=-m_-}^{m_+} \frac{\sin(2n+1)\theta_m}{\cos \theta_m} + \frac{\mathrm{i}(-1)^n}{\kappa d} \left(\sum_{m=0}^{m_+} - \sum_{m=-1}^{-m_-} \right) \frac{\cos(2n+1)\theta_m}{\cos \theta_m}
$$

$$
+ \frac{\mathrm{i}}{\pi} \sum_{m=0}^{n} \frac{(-1)^{m-n}(n+m)! B_{2m+1}(\beta d/\pi)}{(2m+1)!(n-m)!(\kappa d/2\pi)^{2m+1}}
$$

$$
- \frac{\mathrm{i}}{\kappa d} \left[\sum_{m=m_++1}^{\infty} \frac{\mathrm{e}^{-(2n+1)l_m^+}}{\sinh l_m^+} - \sum_{m=m_-+1}^{\infty} \frac{\mathrm{e}^{-(2n+1)l_m^-}}{\sinh l_m^-} \right] \tag{A.2}
$$

and finally,

$$
\mathscr{H}_0 = -1 + \sum_{m=-m_-}^{m_+} \frac{1}{\kappa d \cos \theta_m} - \frac{2\mathrm{i}}{\pi} \left(\gamma + \log \frac{\kappa d}{2\pi} \right) + \mathrm{i} \left(\sum_{m=1}^{m_+} + \sum_{m=1}^{m_-} \right) \frac{1}{m\pi}
$$

$$
- 2\mathrm{i} \sum_{m=m_++1}^{\infty} \left[\frac{1}{\kappa d \sinh l_m^-} - \frac{1}{m\pi} \right] - 2\mathrm{i} \sum_{m=m_-+1}^{\infty} \left[\frac{1}{\kappa d \sinh l_m^-} - \frac{1}{m\pi} \right] \tag{A.3}
$$

where $B_m(x)$ is the Bernoulli polynomial and $m_\pm = [(\mp\beta d + \kappa d)/\pi]$ and $[x]$ denotes the integer part of x. Also

$$
\sin \theta_m = (\beta d + m\pi)/\kappa d, \quad -m_- \leqslant m \leqslant m_+ \tag{A.4}
$$

and

$$
\cosh l_m^\pm = (\pm\beta d + m\pi)/\kappa d, \quad m \geqslant m_+ + 1, \quad \text{and } m \leqslant -m_- - 1 \tag{A.5}
$$

such that all $\theta_m, l_m^\pm$ are real. Here, $\gamma = 0{\cdot}577\ldots$ is Eulers constant.

When $0 \leqslant \kappa d < \beta d < \pi - \kappa d$, it is found that $m_+ = -1$, $m_- = 0$ and all terms in (A.1)–(A.3) containing θ_m's vanish.

Acknowledgement

References

1. R. C. MacCamy and R. A. Fuchs, Wave forces on piles: A diffraction theory. US Army Coastal Engineering Research Center, *Tech. Mem.* 69 (1954).
2. T. H. Havelock, Forced surface waves on water. *Phil. Mag.* 8 (1929) 569-577.
3. C. C. Mei, *The Applied Dynamics of Ocean Surface Waves.* New York: John Wiley and Sons (1983) 740 pp.
4. V. Twersky, Multiple scattering or radiation by an arbitrary configuration of parallel cylinders. *J. Acoust. Soc. America* 24 (1952) 42–46.
5. C. M. Linton and D. V. Evans, The interaction of waves with arrays of vertical circular cylinders. *J. Fluid Mech.* 215 (1990) 549–569.
6. H. Maniar and J. N. Newman, Wave diffraction by long arrays of cylinders. *J. Fluid Mech.* 339 (1997) 309–330.
7. M. Callan, C. M. Linton and D. V. Evans, Trapped modes in two-dimensional waveguides. *J. Fluid Mech.* 229 (1991) 51–64.
8. C. H. Wilcox, *Scattering Theory for Diffraction Gratings*. Berlin: Springer (1984) 163 pp.
9. C. M. Linton and D. V. Evans, Corrigendum: The interaction of waves with arrays of vertical circular cylinders. *J. Fluid Mech.* 218 (1990) 663.
10. D. V. Evans and R. Porter, Near-trapping of waves by circular arrays of vertical cylinders. *Appl. Ocean Res.* 19 (1997) 83–99.
11. P. Gaspard and S. A. Rice, Exact quantization of the scattering from a classically chaotic repellor. *J. Chem. Phys.* 90 (1989) 2255–2262.
12. V. Twersky, Elementary Function Representations of Schlömilch series. *Arch. Rat. Mech.* 8 (1961) 323–332.
13. P. McIver, C. M. Linton and M. McIver, Construction of trapped modes for waveguides and diffraction gratings. *Proc. Roy. Soc. Lond. (A)*, 454 (1998) 2593–2616.
14. C. M. Linton and D. V. Evans, The interaction of waves with a row of circular cylinders. *J. Fluid Mech.* 251 (1993) 687–708.
15. D. V. Evans and M. Fernyhough, Edge waves along periodic coastlines. Part 2. *J. Fluid Mech.* 46 (1995) 644–656.
16. M. McIver and C. M. Linton, On the non-existence or otherwise of trapped modes in acoustic waveguides. *Q. J. Mech. Appl. Math.* 48 (1995) 543–555.
17. D. V. Evans and R. Porter, Trapped modes about multiple cylinders in a channel. *J. Fluid Mech.* 339 (1997) 331–356.
18. D. V. Evans and R. Porter, Trapped modes embedded in the continuous spectrum. *Q. J. Mech. Appl. Math.* 52(2) (1998) 263–274.